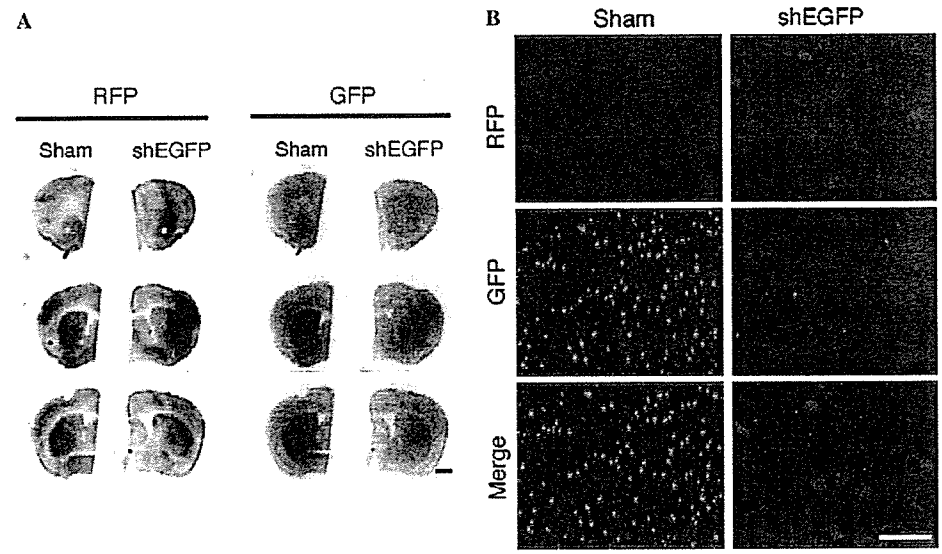

Fig. 2. rAAV-shEGFP transduction in the mouse brain decreases EGFP-positive aggregates (direct observation of EGFP fluorescence). (A) A montage of rostral-to-caudal coronal sections illustrates the extent of expression of RFP and EGFP in the brain. Three microliters of buffer was injected into striatum; sham, and rAAV-shEGFP was simultaneously injected into the contralateral side; shEGFP. Dark areas show fluorescent signal. Scale bar is 1 mm and refers to all panels. (B) EGFP fluorescence of the shEGFP-transduced striatum in high magnification. EGFP fluorescence was directly observed, while RFP was detected by anti-RFP because of the weak fluorescence after fixation. Scale bar is 20 μm and refers to all panels.

detect nuclear aggregates as well as cytoplasmic aggregates, and ubiquitin antibody detects large nuclear aggregates in HD190QG and R6/2 HD transgenic mice [10,21,25]. Reduction of aggregates is one of the indicators for the improvement of pathology in the HD mouse model [9,10,17,19]. In the HD190QG transgenic mouse, aggregate formation was first observed in the striatum at 4 weeks of age. Then, tremor, ataxia, and involuntary movements were observed at 6 weeks [21]. The shRNA was delivered to the striatum in 12 weeks old HD190QG mice to investigate the RNAi effects on disease pathology. At 24 weeks, mice brains were prepared for histological study. Immunohistochemistry was performed using antibodies against GFP, htt, and ubiquitin (Fig. 3A). The number of aggre-

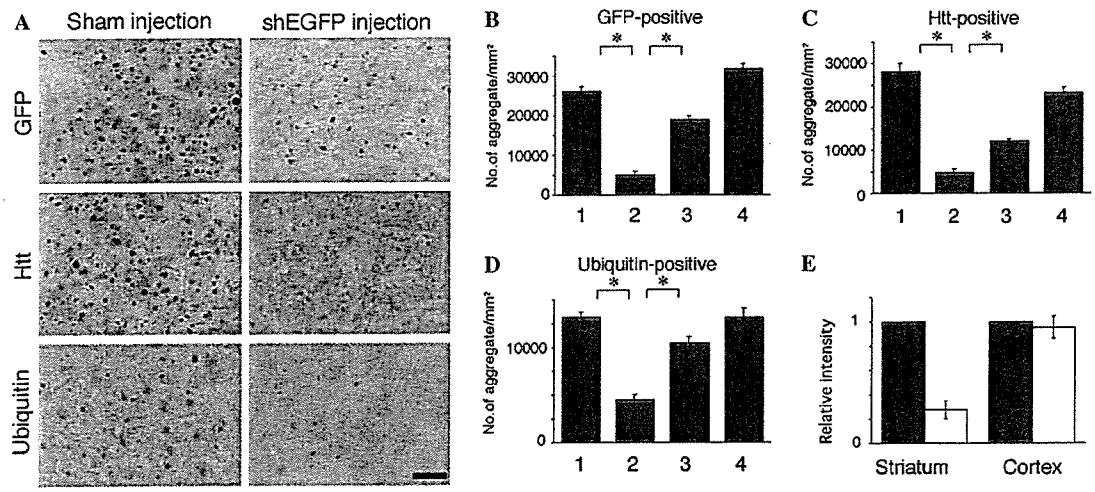

Fig. 3. shEGFP decreased antibody-positive aggregates and ameliorated aggregation pathology. (A) Representative images show GFP-, htt-, and ubiquitin-positive aggregates in the sham-injected or shEGFP-transduced striatum. Scale bar is 20 μm and refers to all panels. (B–D) Number of aggregates in the striatum is shown. rAAV-shEGFP was injected into the striatum at 12 weeks old and analyzed at 24 weeks old. The bars indicate aggregate number in the sham-injected striatum at 24 weeks old (1), shEGFP-transduced striatum at 24 weeks old (2), non-treated 12 weeks old HD190QG striatum, at the time point of shRNA transduction (3), and non-treated 24 weeks old HD190QG, as non-treatment control (4). The graphs show the number of GFP-positive aggregates (B), htt-positive aggregates (C), and ubiquitin-positive aggregates (D). Data are shown as average ± SEM (*Y* axis indicates the number of aggregates/mm^2. Sham-injected, shEGFP-transduced, and 12 weeks old control striatum; $n = 3$, 24 weeks old control striatum; $n = 4$). $^*p < 0.0001$. (E) Quantitative analysis of filter trap assay indicates relative amount of insoluble protein in the treated striatum. The relative fluorescence levels of sham-injected side (black) and shEGFP-transduced side (white) are shown as the average ± SEM ($n = 4$). $^*p < 0.0001$.

gates in the shEGFP-transduced striatum was much reduced than that in sham-injected striatum. The number of GFP-positive aggregates in shEGFP-transduced striatum was decreased to 19.4% of GFP-positive aggregates in sham injection striatum (Fig. 3B, bars 1 and 2). The number of htt-positive aggregates in shEGFP-transduced striatum was reduced to 17.7% of sham injection (Fig. 3C, bars 1 and 2), and the number of ubiquitin-positive aggregates in shEGFP-transduced striatum was reduced to 34.1% of sham injection (Fig. 3D, bars 1 and 2).

Furthermore, the number of aggregates in shEGFP-transduced striatum was significantly less than the number of aggregates formed in the striatum at the same age of shEGFP-transduction (Figs. 3B–D, bars 2 and 3). In this study, shEGFP-transduction was performed at 12 weeks old. The number of aggregate in shEGFP-transduced striatum at 24 weeks old was compared to that in 12 weeks old transgenic mice. The number of GFP-positive aggregates in shEGFP-transduced striatum was decreased to 26.8% of GFP-positive aggregates in 12 weeks old transgenic mice striatum (Fig. 3B, bars 2 and 3). The number of htt-positive aggregates in shEGFP-transduced striatum was reduced to 41.1% of 12 weeks old transgenic mice striatum (Fig. 3C, bars 2 and 3), and the number of ubiquitin-positive aggregates in shEGFP-transduced striatum was reduced to 42.9% of 12 weeks old transgenic mice striatum (Fig. 3D, bars 2 and 3). These results suggest that shEGFP was effective not only for inhibition of aggregation formation but also for clearance of aggregates that already existed in the nucleus and cytoplasm. The number of aggregates in the sham injection site was similar to that in the 24 weeks old transgenic mouse (Figs. 3B–D, bars 1 and 4). This result certifies that the injection procedure did not affect aggregation formation in the striatum. The number of aggregates was also not affected by rAAV-shEGFPcontrol transduction (data not shown).

We further investigated the effect of shEGFP on the accumulation of insoluble protein in the brain. In the HD190QG mouse brain, insoluble proteins including intra- and extra-nuclear aggregates increased in an age-dependent manner [21]. Filter trap assays revealed that insoluble protein accumulation was significantly suppressed in the shEGFP-transduced region compared to that in the sham-treated striatum, whereas it was not changed in the cortex. The reduction was 73% in the striatum and 5% in the cortex (Fig. 3E). Similar results were also obtained using htt antibody (data not shown).

Restoration of DARPP-32 expression by shRNA

To investigate the effect of shEGFP on striatal-specific transcripts, we first performed in situ hybridization using DARPP-32 probe, because DARPP-32 is known to be down-regulated in HD mouse [21,26]. We found the tendency of restored expression of DARPP-32 (Fig. 4A). Thus, we carried out the quantitative TaqMan RT-PCR analysis and confirmed that DARPP-32 and enkephalin mRNA expression was higher in the shEGFP-transduced striatum than the sham-injected side (Fig. 4B), suggesting that those gene expressions were partially restored.

Discussion

In this study, we demonstrated that neuropathological abnormalities associated with HD, such as insoluble protein accumulation and down-regulation of DARPP-32 expression, were successfully ameliorated by RNAi transduction. Following shRNA transduction, the number of neuronal aggregates in the striatum detected by ubiquitin antibody was reduced to 34.1% of that in the sham-treated striatum. Importantly, the number of aggregates in the shEGFP-transduced striatum was less than that in the striatum at the same time point of RNAi transduction.

Various treatments have shown an improvement of HD-associated abnormalities including pathological and behavioral deficits in a mouse model of HD [9,10,27–30]. Most treatments targeted downstream and possibly indirect effect of disease allele of htt, resulting in the delayed disease progression. Silencing of mutant gene expression was demonstrated using a conditional mouse model of HD [20]. Inhibition of mutant gene expression provides a direct approach to treat neurodegenerative diseases caused by toxic gain of function. RNAi is promising as a powerful tool for targeting gene knockdown. The silencing effect of synthesized siRNA injection was sustained more than 14 days in the newborn mouse brain to delay onset and prolong the life span of R6/2 [19]. In contrast, vector-based RNAi stably persisted more than 2–5 months after transduction, resulting in the improvement of motor dysfunction and neuropathological abnormalities [17,18]. AAV5 is efficient to transduce neuronal cells in the mouse brain [17,31,32], and shRNA expression by U6 promoter has been reported in mouse striatum [17]. Here we showed a drastic improvement of HD pathology in the mouse brain by rAAV5-mediated delivery of shRNA even the transduction was performed after the pathology appeared.

RNAi-mediated strategy has been performed as a pre-symptomatic treatment in the previous studies. We investigated whether RNAi treatment is functional on the pathology in the HD model after onset of disease. Gene silencing effects were observed at 2 weeks after virus injection in the symptomatic brain (data not shown), and the effect lasted for more than 3 months. Aggregate formation was effectively inhibited by shRNA transduction and the number of aggregates was decreased significantly compared with that in animals at the age of transduction. This result suggests that AAV-mediated delivery of shRNA could realize stable acquired gene knockdown in the transgenic mouse, and aggregate pathology was ameliorated as reported previously [20].

Expression of mutant htt leads to a decreased level of a subset of striatal-specific mRNAs of the HD190QG, R6/2, and R6/1 mouse [18,21,26]. DARPP-32, which is predominantly expressed in striatum, was down-regulated by 50%

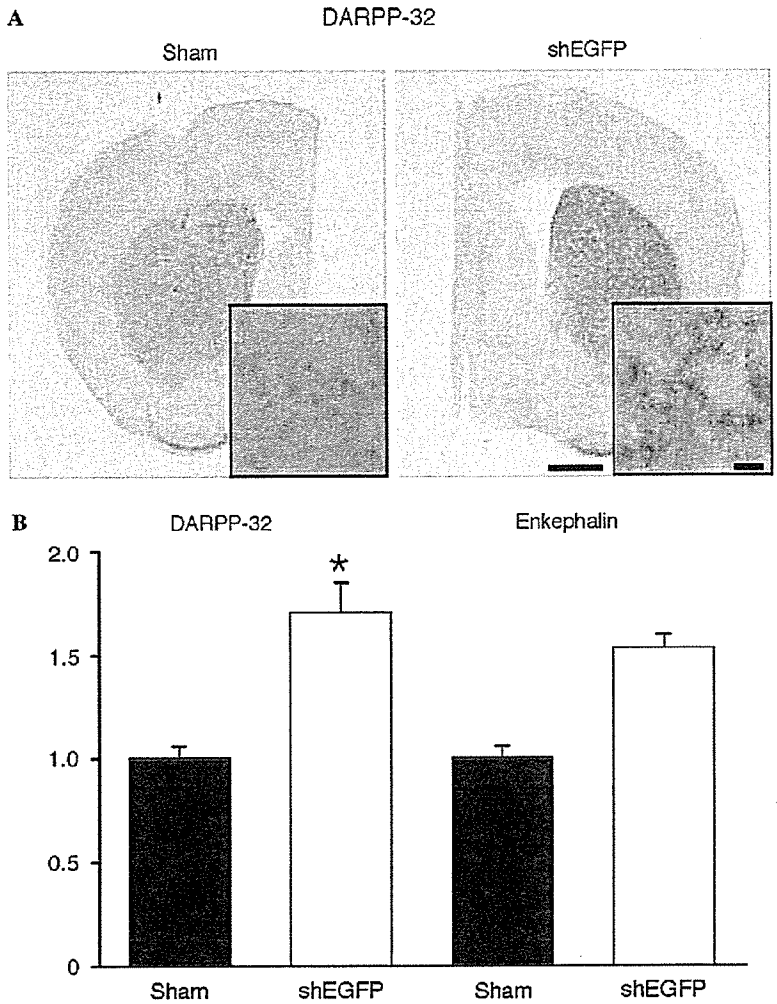

Fig. 4. shRNA restored DARPP-32 and enkephalin expression. (A) In situ hybridization of DARPP-32 at 24 weeks old after rAAV-shEGFP injection into the striatum at 9-week-old. Scale bar shows 1 mm. Higher magnification images of striatum are shown in inset, respectively, and scale bar is 20 μm. (B) DARPP-32 and enkephalin mRNA expression in striatum was determined by TaqMan RT-PCR analysis at 24 weeks after rAAV-shEGFP injection into the striatum performed at 12 weeks old. The expression levels of mRNA were normalized by that of GAPDH. DARPP-32 showed a significant increase in the shEGFP-injected side and enkephalin showed not significant but the tendency to restore. The values are given as means ± SEM ($n = 3$). $^{*}p < 0.05$.

in the 8-week-old HD190QG mouse compared with wild-type [21]. Here, we showed the restoration of DARPP-32 expression. Although the pathology was improved as shown in this report, we could not observe apparent improvement of the symptom or life span in this experiment. This is partly due to the injection was performed only in the one side to confirm the amelioration of the pathology and due to the injection time point, which restricted the full restoration of the function. Further study to determine the critical time of viral transduction for the functional recovery is necessary.

In this study, we used shRNA against EGFP for HD190QG mouse to suppress only the transgene. This shEGFP is designed to modulate mutant htt expression in our animal model but not applicable to the clinical investigation of human HD gene therapy. Although either siRNA or shRNA against htt was produced and investigated previously [17–19], this siRNA sequence reduced not only mutant htt but also wild-type htt simultaneously. Since wild-type htt is essential to embryogenesis, the complete loss of wild-type htt results in embryonic lethality and reduction of wild-type htt leads to behavioral abnormalities and neuronal loss [33]. In fact, loss of wild-type htt in YAC128 mice induced motor dysfunction and survival was worse compared with YAC128 mice expressing wild-type htt [33]. For these reasons, it is required to design a siRNA sequence, which selectively silences mutant htt but not wild-type htt. When a technology is developed to solve this issue, RNAi-based therapy would be practical for pre- and post-symptomatic treatment strategy for HD therapy [15,24].

In summary, we showed that RNAi dramatically improved HD-associated pathological abnormalities in a mouse model of HD, although the treatment was carried out after onset of symptom. Our data suggested that reduction of mutant gene expression by RNAi would be

promising to attenuate disease progression in post-symptomatic neurodegenerative disorders.

Acknowledgments

The authors thank Dr. John A. Chiorini for providing pAAV5-RNL and pAAV5-RepCap (identical to 5RepCapB) and Avigen, Inc. (Alameda, CA) for providing pAAV-LacZ, pHLP19, and pAdeno. We also thank Drs. Nobuhisa Iwata, Takaomi Saido, Mayumi Okada, and Ms. Miyoko Mitsu for their technical supports and Drs. Joanna Doumanis and Hong-Kit Wong for their critical readings. This work was supported in part by grants from Grants-in-Aid for Scientific Research on Priority Areas 17025044 from The Ministry of Education, Culture, Sports, Science and Technology (MEXT) and the Ministry of Health, Labour and Welfare.

References

[1] J.F. Gusella, M.E. MacDonald, Molecular genetics: unmasking polyglutamine triggers in neurodegenerative disease, Nat. Rev. Neurosci. 1 (2000) 109–115.
[2] A.W. Dunah, H. Jeong, A. Griffin, Y.M. Kim, D.G. Standaert, S.M. Hersch, M.M. Mouradian, A.B. Young, N. Tanese, D. Krainc, Sp1 and TAFII130 transcriptional activity disrupted in early Huntington's disease, Science 296 (2002) 2238–2243.
[3] C.J. Cummings, M.A. Mancini, B. Antalffy, D.B. DeFranco, H.T. Orr, H.Y. Zoghbi, Chaperone suppression of aggregation and altered subcellular proteasome localization imply protein misfolding in SCA1, Nat. Genet. 19 (1998) 148–154.
[4] N.R. Jana, M. Tanaka, G. Wang, N. Nukina, Polyglutamine length-dependent interaction of Hsp40 and Hsp70 family chaperones with truncated N-terminal huntingtin: their role in suppression of aggregation and cellular toxicity, Hum. Mol. Genet. 9 (2000) 2009–2018.
[5] U. Nagaoka, K. Kim, N.R. Jana, H. Doi, M. Maruyama, K. Mitsui, F. Oyama, N. Nukina, Increased expression of p62 in expanded polyglutamine-expressing cells and its association with polyglutamine inclusions, J. Neurochem. 91 (2004) 57–68.
[6] H. Doi, K. Mitsui, M. Kurosawa, Y. Machida, Y. Kuroiwa, N. Nukina, Identification of ubiquitin-interacting proteins in purified polyglutamine aggregates, FEBS Lett. 571 (2004) 171–176.
[7] N.F. Bence, R.M. Sampat, R.R. Kopito, Impairment of the ubiquitin-proteasome system by protein aggregation, Science 292 (2001) 1552–1555.
[8] A.V. Panov, C.A. Gutekunst, B.R. Leavitt, M.R. Hayden, J.R. Burke, W.J. Strittmatter, J.T. Greenamyre, Early mitochondrial calcium defects in Huntington's disease are a direct effect of polyglutamines, Nat. Neurosci. 5 (2002) 731–736.
[9] I. Sanchez, C. Mahlke, J. Yuan, Pivotal role of oligomerization in expanded polyglutamine neurodegenerative disorders, Nature 421 (2003) 373–379.
[10] M. Tanaka, Y. Machida, S. Niu, T. Ikeda, N.R. Jana, H. Doi, M. Kurosawa, M. Nekooki, N. Nukina, Trehalose alleviates polyglutamine-mediated pathology in a mouse model of Huntington disease, Nat. Med. 10 (2004) 148–154.
[11] S.M. Elbashir, J. Harborth, W. Lendeckel, A. Yalcin, K. Weber, T. Tuschl, Duplexes of 21-nucleotide RNAs mediate RNA interference in cultured mammalian cells, Nature 411 (2001) 494–498.
[12] J.Y. Yu, S.L. DeRuiter, D.L. Turner, RNA interference by expression of short-interfering RNAs and hairpin RNAs in mammalian cells, Proc. Natl. Acad. Sci. USA 99 (2002) 6047–6052.
[13] A.P. McCaffrey, M.A. Kay, A story of mice and men, Gene Ther. 9 (2002) 1563.
[14] H. Hasuwa, K. Kaseda, T. Einarsdottir, M. Okabe, Small interfering RNA and gene silencing in transgenic mice and rats, FEBS Lett. 532 (2002) 227–230.
[15] G.S. Ralph, P.A. Radcliffe, D.M. Day, J.M. Carthy, M.A. Leroux, D.C. Lee, L.F. Wong, L.G. Bilsland, L. Greensmith, S.M. Kingsman, K.A. Mitrophanous, N.D. Mazarakis, M. Azzouz, Silencing mutant SOD1 using RNAi protects against neurodegeneration and extends survival in an ALS model, Nat. Med. 11 (2005) 429–433.
[16] H. Xia, Q. Mao, S.L. Eliason, S.Q. Harper, I.H. Martins, H.T. Orr, H.L. Paulson, L. Yang, R.M. Kotin, B.L. Davidson, RNAi suppresses polyglutamine-induced neurodegeneration in a model of spinocerebellar ataxia, Nat. Med. 10 (2004) 816–820.
[17] S.Q. Harper, P.D. Staber, X. He, S.L. Eliason, I.H. Martins, Q. Mao, L. Yang, R.M. Kotin, H.L. Paulson, B.L. Davidson, RNA interference improves motor and neuropathological abnormalities in a Huntington's disease mouse model, Proc. Natl. Acad. Sci. USA 102 (2005) 5820–5825.
[18] E. Rodriguez-Lebron, E.M. Denovan-Wright, K. Nash, A.S. Lewin, R.J. Mandel, Intrastriatal rAAV-mediated delivery of anti-huntingtin shRNAs induces partial reversal of disease progression in R6/1 Huntington's disease transgenic mice, Mol. Ther. 12 (2005) 618–633.
[19] Y.L. Wang, W. Liu, E. Wada, M. Murata, K. Wada, I. Kanazawa, Clinico-pathological rescue of a model mouse of Huntington's disease by siRNA, Neurosci. Res. (2005).
[20] A. Yamamoto, J.J. Lucas, R. Hen, Reversal of neuropathology and motor dysfunction in a conditional model of Huntington's disease, Cell 101 (2000) 57–66.
[21] S. Kotliarova, N.R. Jana, N. Sakamoto, M. Kurosawa, H. Miyazaki, M. Nekooki, H. Doi, Y. Machida, H.K. Wong, T. Suzuki, C. Uchikawa, Y. Kotliarov, K. Uchida, Y. Nagao, U. Nagaoka, A. Tamaoka, K. Oyanagi, F. Oyama, N. Nukina, Decreased expression of hypothalamic neuropeptides in Huntington disease transgenic mice with expanded polyglutamine-EGFP fluorescent aggregates, J. Neurochem. 93 (2005) 641–653.
[22] R.E. Campbell, O. Tour, A.E. Palmer, P.A. Steinbach, G.S. Baird, D.A. Zacharias, R.Y. Tsien, A monomeric red fluorescent protein, Proc. Natl. Acad. Sci. USA 99 (2002) 7877–7882.
[23] T. Okada, K. Shimazaki, T. Nomoto, T. Matsushita, H. Mizukami, M. Urabe, Y. Hanazono, A. Kume, K. Tobita, K. Ozawa, N. Kawai, Adeno-associated viral vector-mediated gene therapy of ischemia-induced neuronal death, Methods Enzymol. 346 (2002) 378–393.
[24] T. Okada, T. Nomoto, T. Yoshioka, M. Nonaka-Sarukawa, T. Ito, T. Ogura, M. Iwata-Okada, R. Uchibori, K. Shimazaki, H. Mizukami, A. Kume, K. Ozawa, Large-scale production of recombinant viruses by use of a large culture vessel with active gassing, Hum. Gene Ther. 16 (2005) 1212–1218.
[25] S.W. Davies, M. Turmaine, B.A. Cozens, M. DiFiglia, A.H. Sharp, C.A. Ross, E. Scherzinger, E.E. Wanker, L. Mangiarini, G.P. Bates, Formation of neuronal intranuclear inclusions underlies the neurological dysfunction in mice transgenic for the HD mutation, Cell 90 (1997) 537–548.
[26] R. Luthi-Carter, A. Strand, N.L. Peters, S.M. Solano, Z.R. Hollingsworth, A.S. Menon, A.S. Frey, B.S. Spektor, E.B. Penney, G. Schilling, C.A. Ross, D.R. Borchelt, S.J. Tapscott, A.B. Young, J.H. Cha, J.M. Olson, Decreased expression of striatal signaling genes in a mouse model of Huntington's disease, Hum. Mol. Genet. 9 (2000) 1259–1271.
[27] R.J. Ferrante, J.K. Kubilus, J. Lee, H. Ryu, A. Beesen, B. Zucker, K. Smith, N.W. Kowall, R.R. Ratan, R. Luthi-Carter, S.M. Hersch, Histone deacetylase inhibition by sodium butyrate chemotherapy ameliorates the neurodegenerative phenotype in Huntington's disease mice, J. Neurosci. 23 (2003) 9418–9427.
[28] R.J. Ferrante, O.A. Andreassen, B.G. Jenkins, A. Dedeoglu, S. Kuemmerle, J.K. Kubilus, R. Kaddurah-Daouk, S.M. Hersch, M.F.

Beal, Neuroprotective effects of creatine in a transgenic mouse model of Huntington's disease, J. Neurosci. 20 (2000) 4389–4397.

[29] M. Chen, V.O. Ona, M. Li, R.J. Ferrante, K.B. Fink, S. Zhu, J. Bian, L. Guo, L.A. Farrell, S.M. Hersch, W. Hobbs, J.P. Vonsattel, J.H. Cha, R.M. Friedlander, Minocycline inhibits caspase-1 and caspase-3 expression and delays mortality in a transgenic mouse model of Huntington disease, Nat. Med. 6 (2000) 797–801.

[30] M.V. Karpuj, M.W. Becher, J.E. Springer, D. Chabas, S. Youssef, R. Pedotti, D. Mitchell, L. Steinman, Prolonged survival and decreased abnormal movements in transgenic model of Huntington disease, with administration of the transglutaminase inhibitor cystamine, Nat. Med. 8 (2002) 143–149.

[31] C. Burger, O.S. Gorbatyuk, M.J. Velardo, C.S. Peden, P. Williams, S. Zolotukhin, P.J. Reier, R.J. Mandel, N. Muzyczka, Recombinant AAV viral vectors pseudotyped with viral capsids from serotypes 1, 2, 5 display differential efficiency and cell tropism after delivery to different regions of the central nervous system, Mol. Ther. 10 (2004) 302–317.

[32] M.Y. Mastakov, K. Baer, R.M. Kotin, M.J. During, Recombinant adeno-associated virus serotypes 2- and 5-mediated gene transfer in the mammalian brain: quantitative analysis of heparin co-infusion, Mol. Ther. 5 (2002) 371–380.

[33] J.M. Van Raamsdonk, J. Pearson, D.A. Rogers, N. Bissada, A.W. Vogl, M.R. Hayden, B.R. Leavitt, Loss of wild-type huntingtin influences motor dysfunction and survival in the YAC128 mouse model of Huntington disease, Hum. Mol. Genet. 14 (2005) 1379–1392.

ARTICLE

doi:10.1016/j.ymthe.2005.11.010

A Histone Deacetylase Inhibitor Enhances Recombinant Adeno-associated Virus-Mediated Gene Expression in Tumor Cells

Takashi Okada,[1,*] Ryosuke Uchibori,[1] Mayumi Iwata-Okada,[2] Masafumi Takahashi,[3] Tatsuya Nomoto,[1] Mutsuko Nonaka-Sarukawa,[1] Takayuki Ito,[1] Yuhe Liu,[1] Hiroaki Mizukami,[1] Akihiro Kume,[1] Eiji Kobayashi,[3] and Keiya Ozawa[1,2]

[1]*Division of Genetic Therapeutics,* [3]*Division of Organ Replacement Research, Center for Molecular Medicine, and* [2]*Division of Hematology, Department of Medicine, Jichi Medical School, Tochigi 329-0498, Japan*

**To whom correspondence and reprint requests should be addressed at the Division of Genetic Therapeutics, Center for Molecular Medicine, Jichi Medical School, 3311-1 Yakushiji, Minami-Kawachi, Tochigi 329-0498, Japan. Fax: +81 285 44 8675. E-mail: tokada@jichi.ac.jp.*

Available online 4 January 2006

The transduction of cancer cells using recombinant adeno-associated virus (rAAV) occurs with low efficiency, which limits its utility in cancer gene therapy. We have previously sought to enhance rAAV-mediated transduction of cancer cells by applying DNA-damaging stresses. In this study, we examined the effects of the histone deacetylase inhibitor FR901228 on tumor transduction mediated by rAAV types 2 and 5. FR901228 treatment significantly improved the expression of the transgene in four cancer cell lines. The cell surface levels of alpha v integrin, FGF-R1, and PDGF-R were modestly enhanced by the presence of FR901228. These results suggest that the superior transduction induced by the HDAC inhibitor was due to an enhancement of transgene expression rather than increased viral entry. Furthermore, we characterized the association of the acetylated histone H3 in the episomal AAV vector genome by using the chromatin immunoprecipitation assay. The results suggest that the superior transduction may be related to the proposed histone-associated chromatin form of the rAAV concatemer in transduced cells. In the analysis with subcutaneous tumor models, strong enhancement of the transgene expression as well as therapeutic effect was confirmed *in vivo*. The use of this HDAC inhibitor may enhance the utility of rAAV-mediated transduction strategies for cancer gene therapy.

Key Words: histone deacetylase inhibitor, AAV vector, cancer

INTRODUCTION

Recombinant adeno-associated virus (rAAV) has been of considerable interest to developers of clinical gene therapies [1,2]. This is because, unlike adenoviruses, the introduction of AAV vectors has not been associated with significant inflammation either experimentally or clinically [3]. Furthermore, diseases associated with AAV have not been found in human or animal populations. However, the transduction of cancer cells using rAAV occurs with very low efficiency, which limits its utility in gene therapy. Consequently, we have sought to enhance rAAV-mediated transduction of cancer cells by applying DNA-damaging stresses such as γ-rays or anticancer agents [4–6].

An alternative approach to improving the rAAV-mediated transduction of tumor cells may be to enhance transcription in the target cells. One technique to bring about this event may be to apply a histone deacetylase (HDAC) inhibitor, since HDAC inhibitors are known to regulate the transcription of various genes. Significantly, an HDAC inhibitor increases adenovirus-mediated transduction of cancer cell lines because it enhances the levels of the viral receptor on the cell surface [7]. On the other hand, the effects of HDAC inhibitors on rAAV-mediated transduction of tumor cells have not yet been fully elucidated. Treatment with an HDAC inhibitor causes gene expression from a silenced rAAV genome that has been integrated into the host's genome to recover [8]. However, rAAV exists mostly as an extrachromosomal genome rather than as an integrated genome, and this extrachromosomal form is the primary source of rAAV-mediated gene expression [9]. Therefore, the HDAC inhibitor-mediated recovery of expression from the integrated and silenced genome does not reflect a typical situation of rAAV-mediated transduction. Whereas no

1525-0016/$30.00

clear mechanism has been determined for the effect on the episomal vector-mediated expression, the histone deacetylase inhibitor should also contribute to the enhanced transcription before integration occurs.

Here we show that HDAC inhibitors markedly enhance the transgene expression immediately after rAAV-mediated transduction of tumor cells *in vitro* as well as *in vivo*. Our data also suggest that the vector genome in the cells is in the histone-associated chromatin form, which is capable of superior transcription. HDAC inhibitors may improve tumor cell transduction by enhancing the acetylation of the histone-associated chromatin of the rAAV genome.

RESULTS

Effects of FR901228 Treatment on the Transduction of U251MG Cells with rAAV

To analyze whether an HDAC inhibitor can also improve rAAV-mediated gene expression soon after the infection,

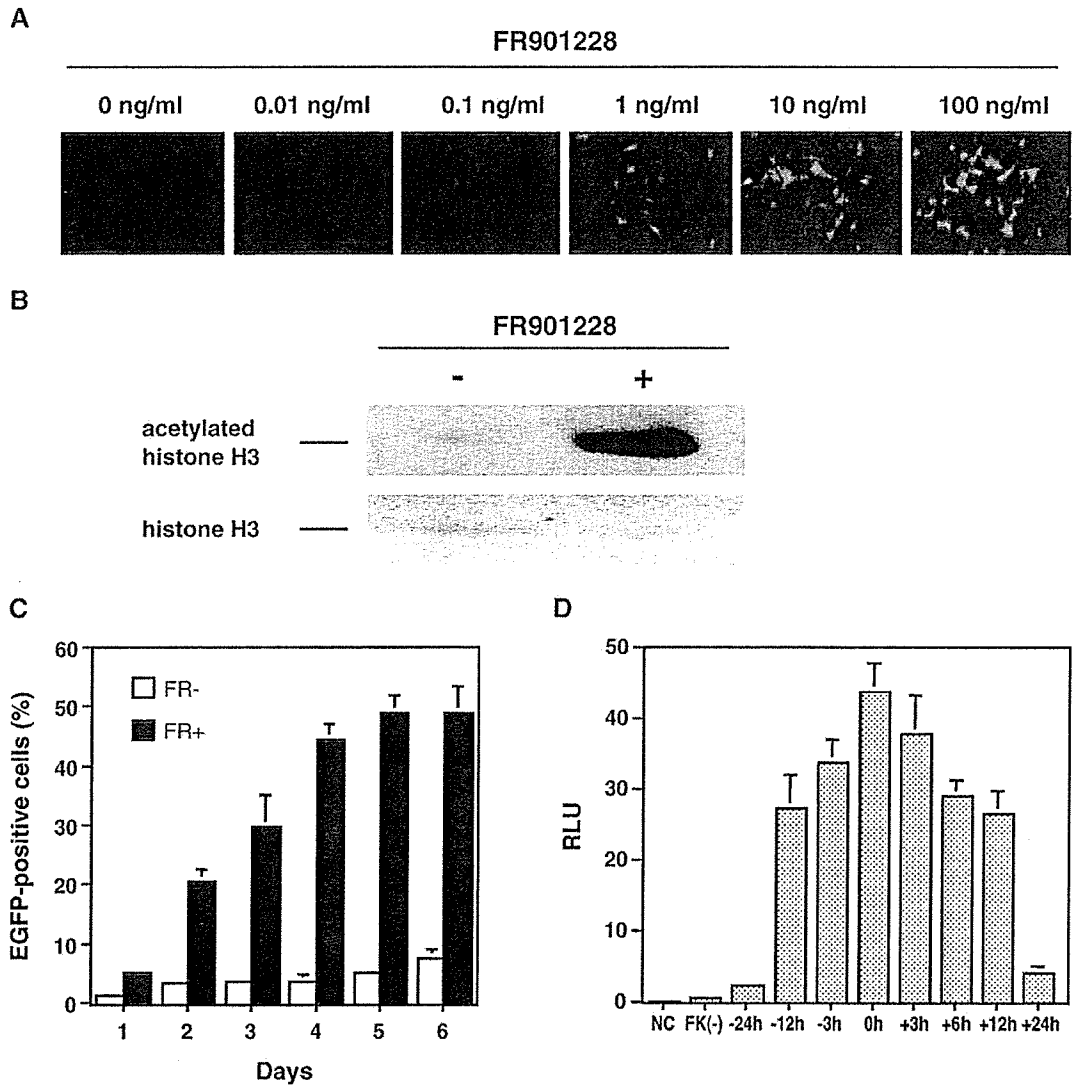

FIG. 1. (A) Effects of FR901228 treatment on the transduction of U251MG cells with rAAV. U251MG cells were infected with 1×10^4 genome copies/cell of AAV2EGFP in the presence of various concentrations of FR901228. EGFP expression was observed 24 h after infection. (B) Detection of the histone acetylation in U251MG cells caused by FR901228 treatment. Cells were incubated in the presence or absence of FR901228 for 24 h. The levels of acetylated histone H3 and histone H3 were determined by Western blot analysis. Histone H3 serves as a loading control. (C) The percentage of EGFP-positive cells at various time points after transduction with AAV2EGFP in the presence (FR+) or absence (FR−) of 1 ng/ml FR901228 was determined by FACS. Cells were infected with AAV2EGFP at 1×10^3 genome copies/cell. The data shown are the means and standard deviations of three independent experiments. (D) The kinetics of the effect on the FR901228-assisted transduction of U251MG cells. Cells were treated with FR901228 at various time points around the transduction with rAAV expressing luciferase as indicated. Luciferase assay was performed on the luminometer 48 h after the transduction.

doi:10.1016/j.ymthe.2005.11.010

we transduced U-251MG human glioma cells with EGFP-expressing rAAV (AAV2EGFP) in the presence of the HDAC inhibitor FR901228. We found that FR901228 treatment improved the AAV2EGFP-mediated gene expression in a dose-dependent manner early after the infection (Fig. 1A). The fact that FR901228 also enhanced the acetylation of the histones in the cells was confirmed by Western blot analysis (Fig. 1B). To assess when gene expression was maximal, we transduced U251MG cells with AAV2EGFP in the presence or absence of 1 ng/ml FR901228 and assessed EGFP expression at various time points after transduction (Fig. 1C). This revealed that the enhancement of gene expression depended on the incubation period and required 4 days before the expression reach a plateau. To analyze the kinetics of the effect on the FR901228-assisted transduction of U251MG cells, cells were treated with FR901228 at various time points around the transduction with luciferase-expressing rAAV type 2 (AAV2-Luc) (Fig. 1D). As a result, the transduction efficiency peaked when cells were treated with FR901228 at the time of virus transduction.

TABLE 1: Relative expression of FGF-R1 and PDGF-R in U251MG cells treated with recombinant AAV alone (1×10^4 genome copies/cell) or together with FR901228 (0.3 or 3 ng/ml) for 24 h as analyzed by quantitative PCR

	$2^{\text{correctedΔCt (GAPDH – target)}}$	
FR901228 (ng/ml)	FGF-R1	PDGF-Rα
0	1.00	1.00
0.3	1.28	1.77
3	1.60	2.30

The relative expression of the target mRNA was determined as the ratio of the expression in U251MG cells treated with recombinant AAV and FR901228 to that in U251MG cells treated with recombinant AAV alone. Data are means ($n = 5$).

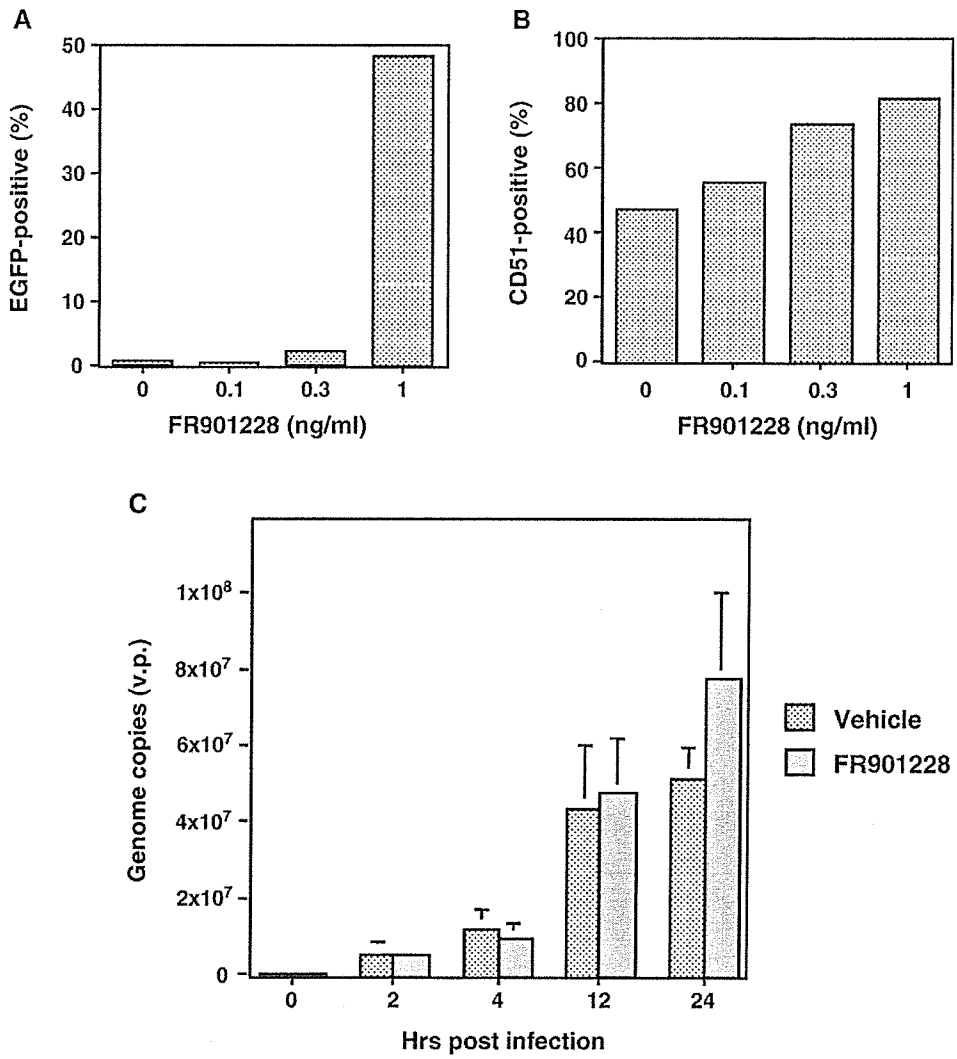

FIG. 2. (A) Percentage of EGFP-positive U251MG cells after transduction with 1×10^4 genome copies/cell of AAV2EGFP in the presence of various concentrations of FR901228. The cells were analyzed 24 h after the transduction for EGFP expression by FACS. The data shown are the average percentages of EGFP-positive cells after three independent transductions. (B) Integrin expression in transduced cells is only modestly enhanced by FR901228 treatment. The cells were stained 24 h after the transduction with monoclonal antibodies to CD51 (integrin v chain, clone 13C2) and analyzed by FACS. The data shown are the average percentages of positive cells after three independent transductions. (C) Transgene copy number in U251MG cells transduced with 1×10^4 genome copies/cell of AAV2EGFP in the presence of 1 ng/ml FR901228. The copy number of the transgene was estimated by real-time PCR at 0, 2, 4, 12, and 24 h after the rAAV infection.

Effects on Receptor Expression and Viral Entry

To determine if FR901228 acted by enhancing the entry of rAAV, we infected U251MG cells with AAV2EGFP in the presence of various concentrations of FR901228 and then analyzed the EGFP and alpha v integrin levels in the cells by fluorescence-activated cell sorting (FACS). This analysis showed that 24 h after AAV2EGFP infection with 1 ng/ml FR901228, 48% of the U251MG cells were EGFP-positive, whereas at lower concentrations of FR901228 only very few cells were EGFP-positive (Fig. 2A). However, this FR901228 concentration range (0.3–1 ng/ml) only modestly enhanced the levels of AAV2 coreceptor, alpha v integrin (Fig. 2B). In addition, when we estimated the amount of the rAAV genome in the transduced cells by real-time quantitative PCR analysis, we found that FR901228 treatment did not significantly affect the copy number of the rAAV (Fig. 2C). Furthermore, we also estimated the effect of FR901228 on the expression of coreceptors for the AAV. FR901228 moderately

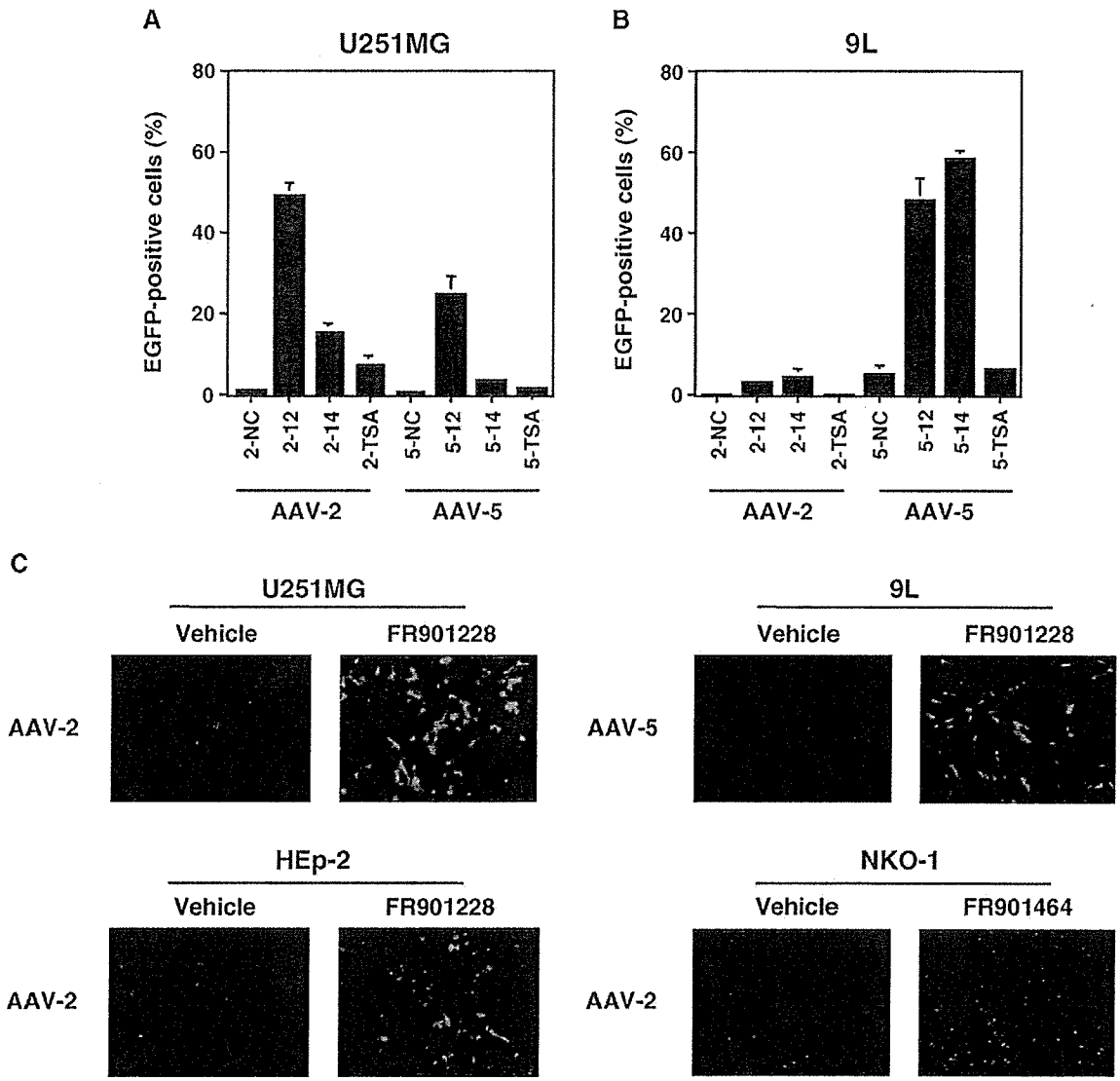

FIG. 3. (A, B) EGFP expression by AAV2EGFP and AAV5EGFP differs depending on the tumor cell being transduced. U251MG or 9L cells were infected with 1×10^4 genome copies/cell of AAV2EGFP (2) or AAV5EGFP (5) in the presence of vehicle (NC) or 1 ng/ml of various HDAC inhibitors, FR901228 (12), FR901464 (14), or TSA. The cells were analyzed by FACS 24 h after the infection. The data show the average percentages of EGFP-positive cells after three independent transductions + SD. (C) Representative data of the enhanced transgene expression by HDAC inhibitors in various cell lines infected with AAV vectors. Twenty-four hours after the AAV2EGFP or AAV5EGFP infection at 1×10^4 genome copies/cell with 1 ng/ml of the FR901228 or FR901464, cells were examined under the fluorescence microscope.

doi:10.1016/j.ymthe.2005.11.010

increased mRNA levels of fibroblast growth factor receptor 1 (FGF-R1) and platelet-derived growth factor receptor (PDGF-R), although the augmentation was not enough to explain the drastic increase of the expression (Table 1).

Transduction of Tumor Cells with AAV Vectors Derived from Distinct Serotypes

Type 2 and type 5 rAAV differed from each other in the efficiency of their transduction of U251MG and the 9L glioma cells. Although FR901228 and other HDAC inhibitors (FR901464 or trichostatin A (TSA)) remarkably enhanced the transduction of both rAAVs in general, AAV2EGFP-mediated transduction of U251MG cells was more efficient than AAV5EGFP-mediated transduction while AAV5EGFP-mediated transduction of 9L cells was better than AAV2EGFP-mediated transduction (Figs. 3A and 3B). FR901228 and FR901464 also had promoting effects on AAV2EGFP- and AAV5EGFP-mediated transduction of the head and neck cancer cell lines HEp-2 and NKO-1 (Fig. 3C).

Chromatin Modification with FR901228

We characterized chromatin composition of the episomal AAV vector genome by using the chromatin immunoprecipitation (ChIP) assay. ChIP is a technique to test for the presence of certain DNA-binding proteins that might modulate chromatin structure and/or transcriptional characteristics of the specific region of DNA with which they are associated. We made use of polyclonal antibodies generated against histone H3 as well as acetylated histone H3, which have been linked to chromatin modification and regulation of transcription. The primers for the CMV promoter region in the AAV vector genome gave a higher level of PCR product when used on templates from FR901228-treated cells compared to those from cells without FR901228 treatment. Higher levels of acetylated histone H3 were found on the CMV promoter region of the AAV vector versus the GAPDH promoter region of the cellular DNA (Table 2A). In contrast, enrichment of acetylated histone H3-associated DNA was not significant on plasmid vector genome irrespective of the presence of the ITR (Table 2B).

FR901228-Assisted Enhancement of Tumor Transduction *in Vivo*

In the analysis using optical bioluminescence imaging of the subcutaneous tumors, we confirmed drastic enhancement of the luciferase gene expression *in vivo* (Fig. 4A). The signal intensity in animals treated with FR901228 (n = 5, [1.5 ± 0.9] × 10^6 photons/s/cm^2/sr) was 37.4-fold higher than in control animals (n = 3, [4.0 ± 2.4] × 10^4 photons/s/cm^2/sr). A subcutaneous

TABLE 2: PCR amplification of immunoprecipitated DNA

(A) Chromatin composition of episomal AAV vector genome was characterized by using the chromatin immunoprecipitation assay

Ab of interest	FR901228	$2^{\text{correctedΔCt (GAPDHprom – CMVprom)}}$
Rabbit IgG	–	<0.001
Rabbit IgG	+	<0.001
Anti-histone H3	–	1.0 ± 1.8
Anti-histone H3	+	7.3 ± 1.4
Anti-acetyl histone H3	–	1.0 ± 0.4] < 0.0001
Anti-acetyl histone H3	+	22.0 ± 0.8]

(B) Cells were transfected with a plasmid harboring the EGFP expression cassette under the CMV promoter (pEGFP) or a plasmid carrying an identical EGFP expression cassette flanked by ITR regions (pITR-EGFP)

Plasmid	Ab of interest	FR901228	$2^{\text{correctedΔCt (GAPDHprom – CMVprom)}}$
pEGFP	Rabbit IgG	–	<0.001
	Rabbit IgG	+	<0.001
	Anti-acetyl histone H3	–	1.0
	Anti-acetyl histone H3	+	1.3
pITR-EGFP	Rabbit IgG	–	<0.001
	Rabbit IgG	+	<0.001
	Anti-acetyl histone H3	–	1.0
	Anti-acetyl histone H3	+	1.2

U251MG cells were transduced with AAV vector at 1 × 10^4 genome copies/cell in the presence or absence of 1 ng/ml FR901228. Twenty-four hours after the transduction, chromatin proteins of interest were cross-linked to DNA by formaldehyde. Shared DNA was immunoprecipitated with histone H3 antibody or acetylated histone H3 antibody to enrich for the CMV promoter region or GAPDH promoter region. Relative differences in the levels of immunoprecipitated DNA, which are reflective of the levels of the chromatin protein of interest occupying a particular island, between different promoter regions and cell treatment with FR901228 were quantified by quantitative PCR.

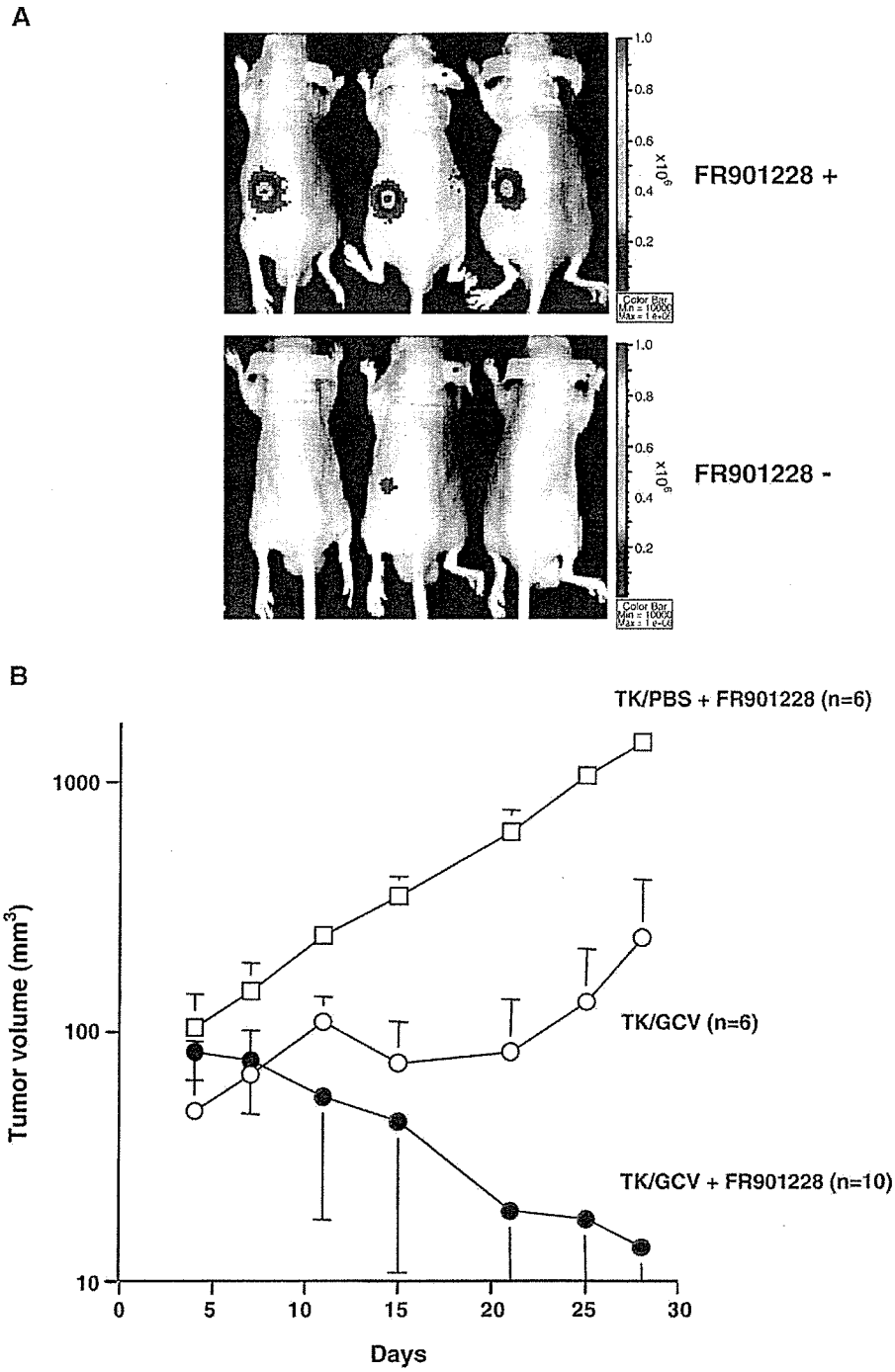

FIG. 4. (A) FR901228-assisted enhancement of tumor transduction *in vivo*. U251MG cells were mixed with PBS (FR901228–, $n = 3$) or transduced with a recombinant AAV2 expressing luciferase (AAV2Luc) at 1×10^4 genome copies/cell for 1 h (FR901228+, $n = 5$), and then 3×10^6 of the transduced cells in 100 μl PBS were inoculated subcutaneously into the BALB/c mice along with the intraperitoneal injection of FR901228 at 1 mg/kg. Twenty-four hours after administration of the FR901228, optical bioluminescence imaging was performed using the CCD camera. (B) The effects of FR901228 on the rAAV-mediated transduction for 9L tumor elimination *in vivo*. Cells were transduced with AAV5TK at 1×10^4 genome copies/cell for 1 h, and then 3×10^6 of the transduced cells in 100 μl PBS containing 25% (v/v) basement membrane matrix were inoculated subcutaneously into the BALB/c mice. The tumor-bearing animals received intraperitoneal injection of FR901228 at 3 mg/kg (group 1, $n = 6$; group 3, $n = 10$) or PBS (group 2, $n = 6$). The animals were also exposed to ganciclovir (GCV) at 100 mg/kg per day (groups 2 and 3) or PBS (group 1) for 14 consecutive days by intraperitoneal placement of the miniosmotic pumps.

tumor model with athymic nude mice demonstrated that the combination of AAV-mediated transduction for HSV-*tk*/GCV therapy and FR901228 treatment ($n = 10$) resulted in statistically significant reduction of tumor growth relative to HSV-*tk*/GCV therapy without FR901228 treatment (unpaired t test, $P < 0.05$, $n = 6$; Fig. 4B). When the tumor-bearing animals were treated with GCV and FR901228, 8 of 10 tumors were eliminated at 4 weeks after transduction.

Discussion

HDAC inhibitors significantly improved the expression of the transgene in cancer cells. The enhancement of the coreceptor level was modest and copy number of the

doi:10.1016/j.ymthe.2005.11.010

rAAV in the transduced cells was also modestly affected by the FR901228 treatment. Furthermore, association of the acetylated histone H3 in the episomal AAV vector genome was demonstrated by using the chromatin immunoprecipitation assay. In the analysis with the subcutaneous tumor models, strong enhancement of the transgene expression as well as therapeutic effect was confirmed *in vivo*.

Treatment with an HDAC inhibitor is known to cause the recovery of the gene expression of a rAAV vector genome that has been integrated and silenced after long-term selection [8]. However, rAAV occurs mostly as extrachromosomal genomes rather than as integrated genomes, and these extrachromosomal forms are the primary source of rAAV-mediated gene expression early after transduction [9]. There has been no direct investigation of the effects of HDAC inhibitors on the rAAV-mediated transient gene expression. We examined whether the HDAC inhibitor could contribute to the enhanced transcription before integration occurs.

FR901228 treatment significantly improved the transient expression of the transgene in four cancer cell lines. The FR901228 treatment improved the rAAV-mediated gene transfer in a dose-dependent manner, and the highest enhancement was observed in the U251MG cells with AAV2EGFP. In the U251MG cells, the cell surface levels of alpha v integrin, FGF-R1, and PDGF-R were only modestly enhanced by the presence of FR901228. These observations contrast with a previous report that suggested that FR901228 enhanced adenovirus transduction by increasing CAR and v integrin RNA levels, thereby enhancing viral entry [7]. However, their study did not demonstrate that these increased RNA levels were associated with increased protein levels or kinetics. In our study, a kinetic analysis of the effect on the FR901228-assisted AAV-mediated transduction of U251MG cells showed that the transduction efficiency peaked when cells were treated with FR901228 at the time of transduction. This is in sharp contrast to the case of the effect of FR901228 on the enhanced adenovirus-mediated transduction. Since enhanced viral entry into the cell is a primary function of FR901228 regarding improved adenovirus transduction, transduction efficiency of the adenovirus was preferentially enhanced when the cells were pretreated with FR901228 before transduction [10].

Interestingly, we observed that type 2 and type 5 rAAV differed from each other in the efficiency of their transduction of the U251MG and 9L cells. The differences in the transduction efficiency of the AAV vectors derived from distinct serotypes may be due to the fact that each AAV serotype recognizes a different receptor and that different cell types may express different levels of these receptors. Type 2 AAV uses the cell surface heparan sulfate proteoglycan (HSPG) as a receptor [11]. However, cell surface expression of HSPG alone is insufficient for type 2 AAV infection and FGF-R1 is also required as a coreceptor for successful viral entry into the host cell [12]. Type 5 AAV transduction requires 2,3-linked sialic acid [13] as well as PDGF-R [14] for efficient binding and transduction. These observations indicate that optimized expression of a transgene borne by rAAV will require the careful selection of the appropriate vector serotype with respect to the target cell.

Our data also suggest that the use of FR901228 in combination with AAV vector infection may improve viral entry into the cells, but also requires additional mechanisms to benefit the target cells for the efficient transduction. Association of the acetylated histone H3 in the episomal AAV vector genome was characterized by using the chromatin immunoprecipitation assay. Characterization of the chromatin modification in the rAAV genome with FR901228 suggested that improved expression of the transgene depends on the chromatin state of the AAV genome in the infected cells rather than viral entry. These results suggest that the superior transduction induced by HDAC inhibitor treatment is actually due to an enhancement of transgene expression associated with chromatin modification rather than to increased viral entry. Thus, epigenetic regulatory mechanisms may be involved in the HDAC inhibitor-mediated improvement of the transduction of cancer cells with rAAV. The rAAV concatemer may need to be present in a histone-associated chromatin form in the cells before efficient transgene expression can occur.

Our study suggests that the improved rAAV-mediated transduction induced by HDAC inhibitor was due to an enhancement of transgene expression rather than increased viral entry. This phenomenon may be related to the proposed histone-associated chromatin form of the rAAV concatemer in transduced cells. The depsipeptide fermentation product FR901228 is currently being tested in clinical trials as an anti-cancer drug. Therefore, to utilize such a compound to assist rAAV-mediated cancer gene therapy is theoretically and practically reasonable. The use of HDAC inhibitors may enhance the utility of rAAV-mediated transduction strategies for future clinical investigation.

Materials and Methods

Recombinant AAV production. The EGFP expression cassette driven by the CMV promoter was ligated into pAAVLacZ [15] and pAAV5-RNL [16] to form the proviral plasmids pAAV2EGFP and pAAV5EGFP. rAAV types 2 and 5 that express the EGFP gene (AAV2EGFP and AAV5EGFP) were generated using the proviral plasmids. The luciferase expression cassette driven by the CMV promoter in pLNCL [17] was cloned into pAAVLacZ to create pAAV2Luc. A rAAV type 2 that expresses the luciferase gene (AAV2Luc) was generated using pAAV2Luc. Likewise, the HSV-*tk* cDNA contained in the pAVS6TK [18] was subcloned into pAAV5-RNL to create pAAV5TK. A rAAV type 5 that expresses the HSV-*tk* gene driven by the CMV promoter (AAV5TK) was generated using pAAV5TK. Transfection of 293 cells with the proviral plasmid, AAV helper plasmid pAAV2H [15] or pAAV5H [16], and adenoviral helper plasmid pAdeno was performed according to the previously described protocol [19] associated with an

active gassing [20]. The physical titer of the viral stock was determined by dot-blot hybridization with plasmid standards.

HDAC inhibitors. The HDAC inhibitor FR901228 (obtained from Fujisawa Pharmaceutical Co., Ltd.) is a depsipeptide fermentation product from *Chromobacterium violaceum* [21]. FR901228 strongly inhibits the proliferation of tumor cells by arresting cell cycle transition and is now being tested in clinical trials [22]. FR901464 (obtained from Fujisawa Pharmaceutical Co., Ltd.) and TSA (Sigma–Aldrich Corp., St. Louis, MO, USA) are also prepared as HDAC inhibitors [21].

Cells and culture. The malignant human glioma cell line U251MG, the malignant rat glioma cell line 9L, the laryngeal epidermoid carcinoma cell line HEp-2, and the human maxillary sinus cancer cell line NKO-1 were used in this study. Cells were cultured in Dulbecco's modified Eagle medium (D-MEM) supplemented with 10% fetal bovine serum (FBS), 100 units/ml penicillin, and 100 μg/ml streptomycin at 37°C, 5% CO_2. Human embryonic kidney 293 cells were cultured with D-MEM:F12 (1:1 mixture) supplemented with 10% FBS, 100 units/ml penicillin, and 100 μg/ml streptomycin at 37°C, 5% CO_2. Luciferase assay was performed on the luminometer (Fluoroskan Ascent FL, Thermo Labsystems, Beverly, MA, USA) using the Bright-Glo Reagent kit (Promega, Madison, WI, USA).

FACS analysis. Approximately 5×10^4 cells were analyzed on the FACScan (Becton–Dickinson, San Jose, CA, USA) with CellQuest software (Becton–Dickinson). Cells were incubated with a PE-labeled monoclonal antibody (13C2) specific for human integrin v chain (CD51; Cymbus Biotechnology Ltd., Chandlers Ford, UK) for 30 min on ice. The 7-aminoactinomycin-D (Via-Probe; Pharmingen, San Diego, CA, USA)-negative cell fraction, which contains the viable cells, was used to detect EGFP- and/or PE-positive cells.

Western blot analysis. Detection of histone acetylation by FR901228 in U251MG cells was performed as described [7]. Western blot analysis of the cells incubated in the presence or absence of FR901228 for 24 h was performed using either a rabbit polyclonal antibody against histone H3 or one against acetylated histone H3 (Upstate Biotechnology, Lake Placid, NY, USA) diluted 1:2000 in 5% milk. The probed membrane was incubated with an anti-rabbit immunoglobulin horseradish peroxidase-linked antibody and developed by ECL Western blotting detection reagents (Amersham Pharmacia Biotech, Piscataway, NJ, USA).

Determination of transgene copy number. Tumor cells were infected with 1×10^4 genome copies/cell of rAAV in the presence of FR901228. The high-molecular-weight DNA was extracted from the cells (DNA Extraction Kit; Qiagen, Inc., Hilden, Germany) 0, 2, 4, 12, and 24 h later. The copy numbers were determined by quantitative PCR analysis of 100 ng of the DNA by using an ABI Prism 7700 sequence detection system (Applied Biosystems, Foster City, CA, USA) as described in the supplementary information.

mRNA analysis of coreceptors for the AAV. U251MG cells were incubated with recombinant AAV either alone (1×10^4 genome copies/cell) or together with FR901228 (0.3 or 3 ng/ml) for 24 h. mRNA was isolated from the cell culture using an RNeasy mini kit (Qiagen) and reverse-transcribed into a single-stranded cDNA using the SuperScript Preamplification System (Invitrogen, Carlsbad, CA, USA). FGF-R1 or PDGF-R mRNA was quantitated by real-time PCR as described in the supplementary information.

PCR analysis of immunoprecipitated DNA. Chromatin immunoprecipitation was performed following the Upstate Biotechnology ChIP kit protocol. U251MG cells were transduced with AAV vector at 1×10^4 genome copies/cell, pCMV-EGFP, or pAAV2EGFP in the presence or absence of the 1 ng/ml FR901228. Twenty-four hours after the transduction, chromatin proteins of interest were cross-linked to DNA. After preclearing, isotype-antibody control or anti-acetylated histone H3 or anti-histone H3 antibody (Upstate Biotechnology) was added to the sonicated chromatin solution and incubated overnight at 4°C with agitation. Resulting immune complexes were collected by the salmon sperm DNA–protein A agarose slurry. The eluted samples were treated with proteinase K and purified by phenol/chloroform extraction. Precipitated DNAs were analyzed for the vector-derived promoter by quantitative PCR with an ABI Prism 7700 sequence detection system as described in the supplementary information.

In vivo analysis of enhanced transgene expression. U251MG cells were treated with PBS ($n = 3$) or transduced with a recombinant AAV2 expressing luciferase (AAV2Luc) at 1×10^4 genome copies/cell for 1 h ($n = 5$), and then 3×10^6 of the transduced cells in 100 μl PBS containing 25% (v/v) basement membrane matrix (Matrigel; BD Biosciences, Franklin Lakes, NJ, USA) were inoculated subcutaneously into male BALB/c *nu/nu* mice (Clea Japan, Tokyo, Japan) along with intraperitoneal injection of FR901228 at 1 mg/kg or the same volume of vehicle. Twenty-four hours after the administration of FR901228, optical bioluminescence imaging was performed using the CCD camera (Xenogen Corp., Alameda, CA, USA). After intraperitoneal injection of reporter substrate D-luciferin (375 mg/kg body wt), mice were imaged for scans.

To analyze the effect of FR901228 on the enhanced tumor elimination *in vivo*, 9L tumor cells were transduced with an AAV5TK at 1×10^4 genome copies/cell for 1 h, and then 3×10^6 of the transduced cells in 100 μl PBS containing 25% (v/v) Matrigel were inoculated subcutaneously into BALB/c mice. The tumor-bearing animals received an intraperitoneal injection of FR901228 at 3 mg/kg (group 1, $n = 6$; group 3, $n = 10$) or PBS (group 2, $n = 6$). The animals were also exposed to ganciclovir at 100 mg/kg per day (groups 2 and 3) or PBS (group 1) for 14 consecutive days by intraperitoneal placement of the miniosmotic pumps (Alzet, Palo Alto, CA, USA) according to the manufacturer's instructions. Tumor growth was monitored two to three times a week by measuring two perpendicular tumor diameters using calipers and the volumes were calculated as $a \times b^2 \times 0.5$, where a is the length and b is the width of the tumor in millimeters. Animals with tumors larger than 2 cm in diameter were euthanized.

ACKNOWLEDGMENTS

FR901228 and FR901464 were kindly provided by Fujisawa Pharmaceutical Co., Ltd. We thank Avigen, Inc. (Alameda, CA, USA) for providing pAAV2H (identical to pHLP19) and pAdeno. We are also indebted to Dr. John A. Chiorini for providing pAAV5H (identical to 5RepCapB) and pAAV5RNL. We also thank Ms. Miyoko Mitsu for her encouragement and support. This study was supported in part by (1) grants from the Ministry of Health, Labor, and Welfare of Japan, (2) Grants-in-Aid for Scientific Research, (3) a grant from the 21st Century COE Program, and (4) the "High-Tech Research Center" Project for Private Universities, matching fund subsidy, from the Ministry of Education, Culture, Sports, Science, and Technology of Japan.

RECEIVED FOR PUBLICATION SEPTEMBER 20, 2005; REVISED OCTOBER 25, 2005; ACCEPTED NOVEMBER 19, 2005.

APPENDIX A. SUPPLEMENTARY DATA

Supplementary data associated with this article can be found in the online version at doi:10.1016/j.ymthe.2005.11.010.

REFERENCES

1. Carter, B. J. (2004). Adeno-associated virus and the development of adeno-associated virus vectors: a historical perspective. *Mol. Ther.* **10:** 981–989.
2. Okada, T., *et al.* (2002). Adeno-associated virus vectors for gene transfer to the brain. *Methods* **28:** 237–247.
3. Zaiss, A. K., Liu, Q., Bowen, G. P., Wong, N. C., Bartlett, J. S., and Muruve, D. A. (2002). Differential activation of innate immune responses by adenovirus and adeno-associated virus vectors. *J. Virol.* **76:** 4580–4590.
4. Kanazawa, T., *et al.* (2001). Gamma-rays enhance rAAV-mediated transgene expression and cytocidal effect of AAV-HSVtk/ganciclovir on cancer cells. *Cancer Gene Ther.* **8:** 99–106.
5. Kanazawa, T., *et al.* (2003). Suicide gene therapy using AAV-HSVtk/ganciclovir in

doi:10.1016/j.ymthe.2005.11.010

combination with irradiation results in regression of human head and neck cancer xenografts in nude mice. *Gene Ther.* **10:** 51–58.
6. Kanazawa, T., *et al.* (2004). Topoisomerase inhibitors enhance the cytocidal effect of AAV-HSVtk/ganciclovir on head and neck cancer cells. *Int. J. Oncol.* **25:** 729–735.
7. Kitazono, M., Goldsmith, M. E., Aikou, T., Bates, S., and Fojo, T. (2001). Enhanced adenovirus transgene expression in malignant cells treated with the histone deacetylase inhibitor FR901228. *Cancer Res.* **61:** 6328–6330.
8. Chen, W. Y., Bailey, E. C., McCune, S. L., Dong, J. Y., and Townes, T. M. (1997). Reactivation of silenced, virally transduced genes by inhibitors of histone deacetylase. *Proc. Natl. Acad. Sci. USA* **94:** 5798–5803.
9. Nakai, H., Yant, S. R., Storm, T. A., Fuess, S., Meuse, L., and Kay, M. A. (2001). Extrachromosomal recombinant adeno-associated virus vector genomes are primarily responsible for stable liver transduction in vivo. *J. Virol.* **75:** 6969–6976.
10. Vanoosten, R. L., Moore, J. M., Ludwig, A. T., and Griffith, T. S. (2005). Depsipeptide (FR901228) enhances the cytotoxic activity of TRAIL by redistributing TRAIL receptor to membrane lipid rafts. *Mol. Ther.* **11:** 542–552.
11. Summerford, C., and Samulski, R. J. (1998). Membrane-associated heparan sulfate proteoglycan is a receptor for adeno-associated virus type 2 virions. *J. Virol.* **72:** 1438–1445.
12. Qing, K., Mah, C., Hansen, J., Zhou, S., Dwarki, V., and Srivastava, A. (1999). Human fibroblast growth factor receptor 1 is a co-receptor for infection by adeno-associated virus 2. *Nat. Med.* **5:** 71–77.
13. Walters, R. W., *et al.* (2001). Binding of adeno-associated virus type 5 to 2,3-linked sialic acid is required for gene transfer. *J. Biol. Chem.* **276:** 20610–20616.
14. Di Pasquale, G., *et al.* (2003). Identification of PDGFR as a receptor for AAV-5 transduction. *Nat. Med.* **9:** 1306–1312.
15. Okada, T., *et al.* (2001). Development and characterization of an antisense-mediated prepackaging cell line for adeno-associated virus vector production. *Biochem. Biophys. Res. Commun.* **288:** 62–68.
16. Chiorini, J. A., Kim, F., Yang, L., and Kotin, R. M. (1999). Cloning and characterization of adeno-associated virus type 5. *J. Virol.* **73:** 1309–1319.
17. Okada, T., *et al.* (1997). Inhibition of gene expression from the human c-erbB gene promoter by a retroviral vector expressing anti-gene RNA. *Biochem. Biophys. Res. Commun.* **240:** 203–207.
18. Okada, T., *et al.* (2001). AV.TK-mediated killing of subcutaneous tumors in situ results in effective immunization against established secondary intracranial tumor deposits. *Gene Ther.* **8:** 1315–1322.
19. Okada, T., *et al.* (2002). Adeno-associated viral vector-mediated gene therapy of ischemia-induced neuronal death. *Methods Enzymol.* **346:** 378–393.
20. Okada, T., *et al.* (2005). Large-scale production of recombinant viruses using a large culture vessel with active gassing. *Hum. Gene Ther.* **16:** 1212–1218.
21. Nakajima, H., Kim, Y. B., Terano, H., Yoshida, M., and Horinouchi, S. (1998). FR901228, a potent antitumor antibiotic, is a novel histone deacetylase inhibitor. *Exp. Cell Res.* **241:** 126–133.
22. Sandor, V., *et al.* (2002). Phase I trial of the histone deacetylase inhibitor, depsipeptide (FR901228, NSC 630176), in patients with refractory neoplasms. *Clin. Cancer Res.* **8:** 718–728.

Jpn. J. Infect. Dis., 59, 285-293, 2006

Original Article

Biodistribution of a Low Dose of Intravenously Administered AAV-2, 10, and 11 Vectors to Cynomolgus Monkeys

Seiichiro Mori, Takamasa Takeuchi, Yutaka Enomoto, Kazunari Kondo, Kaori Sato, Fumiko Ono[1], Naoko Iwata[2], Tetsutaro Sata[2] and Tadahito Kanda*

Center for Pathogen Genomics and [2]Department of Pathology, National Institute of Infectious Diseases, Tokyo 162-8640, and
[1]Corporation for Production and Research of Laboratory Primates, Ibaraki 305-0843, Japan

(Received May 12, 2006. Accepted June 26, 2006)

SUMMARY: In gene therapy trials, adeno-associated virus (AAV) vectors are injected directly into target tissues such as muscle and liver. Direct injection can lead to the introduction of a low level of the vector into blood circulation. To determine the systemic effects of the vector released in the blood, we extensively examined the biodistribution of intravenously administered AAV serotype 2 (AAV2) vector in cynomolgus monkeys. Although the vector distribution pattern varied from monkey to monkey, the vector DNA was maintained in the various tissues beyond 7 months post-inoculation (pi). The vector DNA was detected in the lymphoid tissues, particularly in the spleen, more frequently and at a much higher level than in the other tissues tested (i.e., brain, lung, liver, heart, gallbladder, pancreas, colon, kidney, ovary, uterus, etc.). The expression of a transgene was detected in the lymph nodes at 3 months pi. The distribution of two pseudotyped vectors, AAV2/10 and AAV2/11, was similar to that of the AAV2 vector. The present results suggest that when introduced intravenously, the AAV vector DNA persists and may induce transgene expression in various monkey tissues. Thus, the possibility of inadvertent gene transfer to various non-target tissues should be considered in a gene therapy strategy with an AAV vector.

INTRODUCTION

Adeno-associated virus (AAV), a nonenveloped small DNA virus belonging to the genus *Dependovirus* of the family *Parvoviridae*, has been engineered for use as a gene-transfer vector in gene therapy (1). Expression of a transgene introduced into target cells by the AAV vector is expected to last for a long period of time. Fundamental methods of AAV vector production, purification, and quality control have been developed by using the human AAV serotype 2 (AAV2) vector as a model system (2). Pseudotyped AAV2 vectors, in which the AAV2 vector genomes are packaged with capsids from AAVs of the other serotypes, have recently been developed (3). Some of the pseudotypes have shown organ tropism that differs from that of the AAV2 vector (3).

The AAV vector genome, which encodes a transgene, is a single-stranded 4.7 kb DNA. At each end of the vector genome is a 145-base region (inverted terminal repeat [ITR]) containing the viral origin of DNA replication and the packaging signal (1). Since the vector genome lacks the viral rep gene, the product of which mediates viral DNA replication and integration of the viral DNA into the AAVS1 region in human chromosome 19, the vector DNA is not replicable and is randomly integrated into host cell chromosomes or is maintained as episomes of the circularized intermediates (4,5). The vector capsid, an icosahedral particle with a diameter of 25 nm, is composed of the AAV capsid proteins (VP1, VP2, and VP3).

Since AAV vectors are highly stable and can infect various organs, AAV vectors are considered to be suitable for in vivo administration. However, the direct injection of an AAV vector into the target tissue leads to the infection of distant non-target tissues with the vector via blood circulation in non-human primates (6-11). The AAV2 vector, when administered by instillation to the bronchial epithelium of rhesus monkeys, is distributed to the heart, liver, jejunum, kidney, lymph nodes, spleen, pancreas, and brain (6). The AAV2 vector, when injected into the liver of rhesus fetuses, is distributed to the lymph node, liver, skin, spleen, lung, and esophagus of human infants (8). The AAV2 vector, when injected into the muscle, is distributed to the liver and lymph nodes (7). Thus, detailed evaluation of vector biodistribution to various tissues is a necessary part of the assessment of the safety of the vector in the context of administering a gene therapy strategy with in vivo administration.

In this study, the biodistribution of intravenously injected AAV2 vectors and pseudotyped AAV2/10 and 2/11 vectors in cynomolgus monkeys was examined in more extensive detail than that of previous studies (6-11). These studies show that the entry of a portion of the vector into the blood vessels is unavoidable after direct inoculation of the vector into the target tissue. Given the doses of AAV vectors used in clinical trials (2×10^{12} genome copies [gc]/kg weight), we chose AAV vector doses of 2×10^{9} gc to 5×10^{10} gc/kg weight for intravenous injection into the monkeys, assuming that 1/100 to 1/1,000 of the inoculate could leak into the bloodstream from the tissue that had received the vector injection. The AAV vector DNA in the tissue samples was measured semi-quantitatively by agarose gel electrophoresis of a PCR-amplified vector DNA. The results were expected to provide basic data required to evaluate the safety of in vivo administration of the AAV vectors.

*Corresponding author: Mailing address: Center for Pathogen Genomics, National Institute of Infectious Diseases, Toyama 1-23-1, Shinjuku-ku, Tokyo 162-8640, Japan. Tel: +81-3-5285-1111 ext. 2524, Fax: +81-3-5285-1166, E-mail: kanda@nih.go.jp

MATERIALS AND METHODS

AAV vectors: The vector genomes used in this study are shown in Figure 1. The FLAG-tagged beta-galactosidase gene (beta-galF) was produced by PCR with the reverse primer possessing a FLAG-tag sequence (5′-GATTACAAGGATG ACGACGATAAG) and previously produced pAAVbeta-gal (12) as the template. The beta-galF was inserted between the cytomegalovirus immediate early enhancer/promoter and SV40 polyA signal to produce the genome of AAV2(beta-galF). The fusion gene of EGFP and human alpha-tubulin (EGFPtub) was obtained from pEGFP-Tub (BD Bioscience Clontech, Palo Alto, Calif., USA) by cleavage with *Nhe*I and *Bam*HI. The EGFPtub was inserted between the human elongation factor 1 alpha (EF1alpha) promoter and SV40 polyA signal to produce the genome of AAV2(EGFPtub). By using PCR G at nucleotide 157 (nt157) (A at the first ATG of the EGFP gene is designated as nt1) was changed to T to produce a novel *Hin*dIII cleavage site to obtain EGFPatub. Similarly, G at nt 129 was changed to T to produce a *Hin*dIII cleavage site to obtain EGFPbtub. The amino acid sequences of EGFPatub and EGFPbtub were not affected by the nt substitutions. Each vector genome was flanked with the ITR sequence of AAV2.

beta-galF or EGFPtub was packaged into the AAV2 capsid in human 293 cells as described previously (12). Similarly, EGFPatub and EGFPbtub were packaged into the AAV10 and AAV11 capsids, respectively. The AAV2 vector stocks used in Experiments I, II, and III (Table 1) were purified by heparin affinity column chromatography (13), and the vector stocks used in Experiment IV were purified by CsCl equilibrium centrifugation (12). The infectivity of the AAV2 vector purified by CsCl centrifugation was comparable to that of the AAV2 vector purified by heparin column chromatography. Extract from 293 cells that had not been transfected with plasmids for vector production was similarly processed by heparin affinity column chromatography and was used as a mock inoculant.

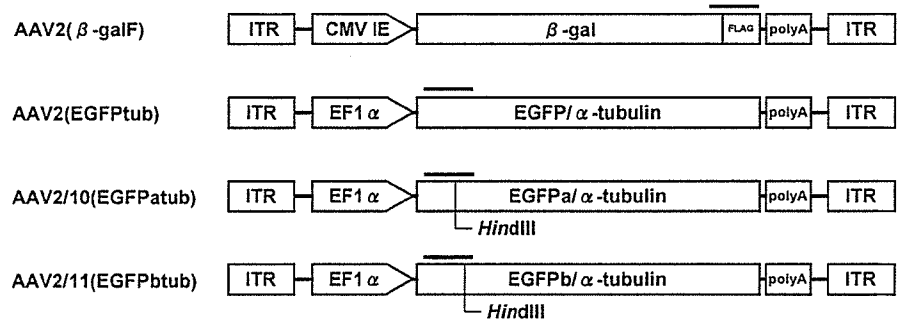

Fig. 1. Schematic representation of the vector genomes. AAV2(beta-galF) is the type 2 vector which has the FLAG-tagged beta-galactosidase gene driven by the cytomegalovirus immediate early promoter (CMV IE). AAV2(EGFPtub) is the type 2 vector which has the fusion gene of enhanced green fluorescent protein (EGFP) and alpha-tubulin driven by the human elongation factor I alpha promotor (EF1 alpha). AAV2/10(EGFPatub) is the type 10 pseudotyped vector which has the fusion gene of EGFPa and alpha-tubulin driven by EF1 alpha. EGFPa has a cleavage site of *Hin*dIII at the nucleotide (nt) 157 (A at the first ATG of EGFP cording region is numbered as nt 1). AAV2/11(EGFPbtub) is the type 11 pseudotyped vector which has the fusion gene of EGFPb and alpha-tubulin driven by EF1 alpha. EGFPb has a cleavage site of *Hin*dIII at the nt 124. The horizontal bars represent PCR amplicons used for detection of the vector genomes. ITR, inverted terminal repeat of AAV2; polyA, SV40 poly adenylation signal.

Table 1. Study design for vector administration in cynomolgus monkeys

Experiment	Monkey No.	Gender	AAV vector	Dose (genome copies/animal)	Time of sample collection
I	#1	FM	Mock	–	2 days
	#2	FM	AAV2(β-galF)	2.5×10^{10}	2 days
	#3	FM	AAV2(β-galF)	2.5×10^{10} [1)]	3 months
	#4	M	AAV2(β-galF)	2.5×10^{10}	3 months
	#5	FM	AAV2(β-galF)	2.5×10^{10}	3 months
II	#6	M	AAV2(EGFPtub)	2.5×10^{11}	3 months
	#7	FM	AAV2(EGFPtub)	2.5×10^{11}	3 months
	#8	M	AAV2(EGFPtub)	2.5×10^{11}	3 months
	#9	FM	AAV2(EGFPtub)	2.5×10^{11}	3 months
III	#10	FM	AAV2(EGFPtub)	1.0×10^{11}	5 months
	#11	FM	AAV2(EGFPtub)	1.0×10^{11}	5 months
	#12	M	AAV2(EGFPtub)	1.0×10^{11}	5 months
	#13	M	AAV2(EGFPtub)	1.0×10^{11}	5 months
IV	#14	FM	Mock	–	3 months
	#15	FM	AAV2, 2/10, 2/11 [2)]	1.0×10^{10} each	3 months
	#16	M	AAV2, 2/10, 2/11	1.0×10^{10} each	3 months
	#17	FM	AAV2, 2/10, 2/11	1.0×10^{10} each	7 months

[1)]: #3 was received second injection of AAV2(beta-galF) (5×10^{10} gc) at 60 days after the first injection.
[2)]: Mixture of AAV2(EGFPtub), AAV2/10(EGFPatub), and AAV2/11(EGFPbtub).

The DNase-resistant vector DNA in the vector stock was measured by Real-Time PCR (Applied Biosystems, Foster City, Calif., USA) with TaqMan probes (CCCAACGAGAAG CGCGATCACA) hybridized to EGFP DNA.

Animal experiments: Cynomolgus monkeys (4 to 5 years of age and weighing 3 to 5 kg) were obtained from the Tsukuba Primate Research Center of the National Institute of Biomedical Innovation (Ibaraki, Japan). The monkeys were sedated during all procedures by the administration of ketamine (10 mg/kg). The AAV vectors or the mock inoculant in 5 ml of physiological saline were administered intravenously into the femoral vein of the monkeys. The dose of the AAV vectors and the time of necropsy are indicated in Table 1. The monkeys were bled every 2 weeks until they were sacrificed. All animal studies were performed in accordance with the guidelines for animal experiments in National Institute of Infectious Diseases, Tokyo, Japan.

Extraction of DNA from tissues: Monkey tissues were harvested at necropsy and stored at −80°C until use. Before necropsy, blood was extensively drawn to avoid contamination of the tissues by blood. DNA was extracted from each frozen tissue type (approximately 25 mg) by using QIAamp DNA extraction kit (Qiagen GmbH, Hilden, Germany).

Detection of AAV vector DNA in tissue DNA: PCR was designed to amplify the 285-bp region of beta-galF (forward primer: 5′-GCGACTTCCAGTTCAACATC, reverse primer: 5′-TTACGCGAAATACGGGCAGA) and 323-bp region of EGFP (forward primer: 5′-ACAAGTTCAGCGTGTCCGGC, reverse primer: 5′-CCTCCTTGAAGTCGATGCCC) in the vector genomes. PCR consisted of an initial heating step at 94°C for 5 min, 37 cycles of incubation at 94°C for 30 s and at 68°C for 1 min, and incubation at 68°C for 5 min. The vector DNA fragment in the tissue DNA sample was amplified by PCR. The DNA sample contained 0.5 μg DNA (equivalent to 10^5 cells). For comparison, the DNA fragment in standard DNA solution, which contained a known amount of plasmid DNA having beta-galF or EGFPtub genes (10^2 to 10^5 copies) and DNA extracted from the liver of monkey (#1) that had received the mock inoculant were amplified by PCR in a similar manner. To verify the quality and quantity of DNA in the samples, a portion of G3PDH gene was amplified with the previously described primers (12). The PCR products were analyzed by electrophoresis on a 2% agarose gel followed by ethidium bromide staining. When the DNA sample contained more than 100 gc of the vector DNA, the amplified DNA fragment was clearly detected (Fig. 2).

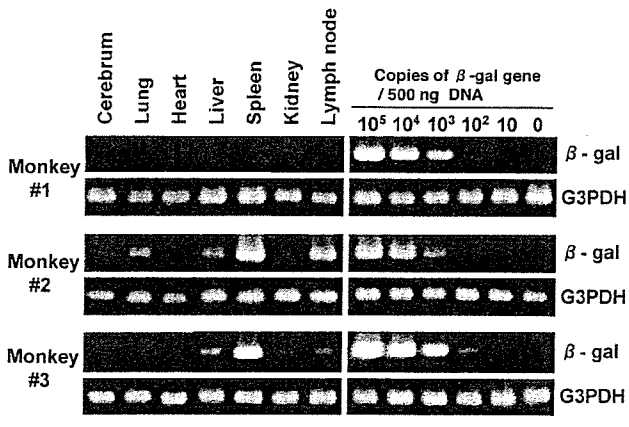

Fig. 2. Detection of AAV vector DNA in monkey tissues. DNA samples were extracted from the various tissues of monkey #1, injected with mock inoculate, and of monkeys #2 and 3, injected with AAV2(beta-galF). The segment of the vector genome in the DNA samples was amplified by PCR. G3PDH gene was amplified for references. Representative results of the agarose gel electrophoresis of the PCR products were presented.

To determine the serotype of the vector in Experiment IV, PCR products were digested with *Hin*dIII, and the size of the resultant DNA fragment was analyzed with an Agilent 2100 Bioanalyzer (Agilent Technologies, Palo Alto, Calif., USA). The *Hin*dIII digestion produced 324-bp, 243-bp, and 276-bp fragments from the genomes of AAV2(EGFPtub), AAV2/10(EGFPatub), and AAV2/11(EGFPbtub), respectively.

Immunoblot detection of EGFP/alpha-tubulin fusion protein in the tissue extracts: Monkey tissue (50 mg) was homogenized in a lysis buffer (0.1M MES, 2 mM EGTA, 1 mM $MgCl_2$, pH 6.8) and the homogenate was centrifuged at 100,000 g for 30 min at 4°C. The supernatant was mixed with Taxol (Paclitaxel; Sigma-Aldrich, St. Louis, Mo., USA) (20 μM) and GTP (Sigma-Aldrich) (0.5 mM), and was warmed to 37°C for 30 min in order to allow the tubulin to assemble into microtubules. Then, the supernatant was chilled on ice for 10 min and was centrifuged at 10,000 × g for 30 min at 4°C to precipitate the microtubules. The pellet was resuspended in PBS and electrophoresed in SDS-polyacrylamide gel. The proteins in the gel were transferred to a Hybond-P nylon membrane (Amersham Biosciences Corp., Piscataway, N.J., USA). After blocking the membrane with 5% skim milk, the EGFP/tubulin fusion protein on the membrane was allowed to bind with anti-EGFP rabbit polyclonal antibody (#632376; BD Bioscience Clontech, Palo Alto, Calif., USA) and anti-alpha-tubulin mouse monoclonal antibody (T-9026; Sigma-Aldrich). Horseradish peroxidase conjugated anti-rabbit and anti-mouse IgG goat antibodies (SC-2030 and SC-2031, respectively; Santa Cruz Biotechnology, Inc., Santa Cruz, Calif., USA) and an ECL Western Blotting Detection System (Amersham Biosciences) were used to detect rabbit and mouse IgGs on the membrane. Fluorescence was detected using a Storm Phosphor Imager (Amersham Biosciences).

A HeLa cell clone expressing EGFPtub was newly produced and used as a model for immunoblot detection of endogenous tubulin and EGFPtub. HeLa cells, cultured in growth medium (DMEM supplemented with 10% fetal bovine serum) in a 10-cm dish, were transfected with 2 μg of pEGFP-Tub (BD Bioscience Clontech) with the transfection reagent Effectene (Qiagen). After incubation of the cells for 48 h, they were passaged at a split ratio of 1 to 10 and cultured in growth medium containing a selective drug, G418 (500 μg/ml). Drug-resistant cell clones were obtained by two successive single colony isolations. One clone (HeLa/EGFPtub) that stably expressed EGFPtub was selected. Endogenous tubulin and EGFPtub were extracted from HeLa/EGFPtub and were used as markers for tubulin and EGFPtub.

Neutralization of AAV vectors with serum antibody: The neutralizing activities of the monkey serum were examined by testing the inhibition of the transduction of COS-1 cells by AAV vectors expressing beta-gal. COS-1 cells (2×10^4 cells/well) were seeded in 96-well plates at 6 h before inoculation. Fifteen microliters of vector solution containing 4×10^3 transducing unit/ml was mixed with 18 μl of serum that had been serially diluted from 1:10 to 1:6,250 with PBS and incubated for 1 h at 37°C. The number of vector genome copies required for 4×10^3 transducing unit with COS-1 were 10^6 gc, 10^8 gc, and 10^8 gc for the AAV2,

AAV2/10, and AAV2/11 vectors, respectively. Then, the sample was mixed with 30 μl of DMEM containing 10% FBS and was used to inoculate the cells in two wells (30 μl/well). After incubation of the cells with occasional rocking for 2 h at 37°C, 70 μl of fresh DMEM containing 10% FBS was added to each well. Two days later, the cells were fixed and stained using an In Situ beta-Galactosidase Staining Kit (Stratagene, La Jolla, Calif., USA). The cells that showed positive staining for beta-gal were counted under a microscope. The neutralizing titer of the antiserum was expressed as the reciprocal of the highest dilution that repressed the number of beta-gal-positive cells to half of the number obtained with the samples mixed with similarly diluted serum from a non-immunized mouse.

RESULTS

Distribution of AAV2(beta-galF) in cynomolgus monkeys: In Experiment I (Tables 1 and 2), one (#1) and four monkeys (#2, 3, 4, and 5) were intravenously injected into the femoral vein with a mock inoculate and 2.5×10^{10} gc of AAV2(beta-galF) (Fig. 1), respectively. No clinical symptoms were observed among these monkeys, indicating that the AAV2 vector particle did not induce any acute toxic effects, as has also been reported previously (4,14). In urine collected between 0 and 24 h post-inoculation (pi), a very low level of the vector DNA was found in monkey #2 sample (10^2 gc/30 μl), but this was not observed in the samples from the other monkeys. The vector DNA was not detected in the urine collected between 24 and 48 h pi from any of the five monkeys. The results indicated that excretion of the injected AAV2 vector was very limited. In whole blood samples obtained at 1 day pi, a very low level of the vector DNA was found in samples from monkeys #2, 3, 4, and 5 (10^2 gc/10 μl). Since the body weight of these monkeys was approximately 3 kg, the total blood of each monkey could be estimated as 250 ml. Therefore, only 1/10,000 of the vectors initially administered is thought to have remained in the circulating blood at 1 day pi. In whole blood samples from monkeys #3, 4, and 5 obtained at 1 week pi, no vector DNA was detected (data not shown).

Monkeys #1 and 2 were sacrificed at 2 days pi. The vector DNA was found in none of the monkey #1 samples, and it was found in various tissues of monkey #2 (Fig. 2 and Table 2). Relatively high levels of the vector DNA were observed in the spleen, tonsil, and axillary lymph node. Low levels of the vector DNA were detected in the brain, ovary, and uterus. Histological examination of formalin-fixed specimens of tissues positive for the vector DNA did not show any abnormalities or inflammatory reactions.

At 2 months pi, monkey #3 received a second intravenous injection with 5×10^{10} gc of AAV2(beta-galF). No clinical symptoms were observed after the injection, indicating that the second injection did not induce any strong acute abnormal immunological reactions.

Monkeys #3, 4, and 5 were sacrificed at 3 months pi. During the 3-month period, the hematological profiles were examined periodically, and no abnormalities were found in the blood samples of monkeys #3, 4, and 5 (data not shown). The vector DNA was present in various tissues (Fig. 2 and Table 2). The highest vector DNA level was detected in the spleen of monkey #3, which had been injected twice with the vector. Among monkeys #3, 4, and 5, the vector distribution pattern to tissues appeared to vary from monkey to monkey. For example, the vector DNA was not detected in the spleen of monkey #5. It was noteworthy that, the vector DNA was found in the ovaries of monkeys #3 and 5, albeit at low levels. The detection of the vector DNA in the spleen, lymph node, and ovary sections by in situ hybridization with PCR was not successful, because it was difficult to find sections positive for the vector DNA. Thus, no vector DNA-positive cell species within the tissues were identified.

Because the vector DNA was readily detected in lymphoid tissues such as the spleen and lymph nodes, we examined the susceptibility of peripheral blood mononuclear cells (PBMCs) to the vector. PBMCs were collected from a cynomolgus monkey that had received no AAV vectors before and were incubated with an AAV2 vector. PBMCs (10^5) or COS-1 cells (5×10^4) in the wells of a 48-well plate were inoculated with 10^9 genome copies of AAV2(EGFP-tub). Three days later, the cells were examined for EGFP expression under a fluorescence microscope. Whereas almost all of the COS-1 cells were positive for EGFP expression, none of the PBMCs were positive for EGFP. It is possible that following the low-dose intravenous injection to the monkeys, the vector did not infect the lymphocytes in the spleen and lymph node.

Table 2. Experiment I: Detection of the vector genomes in the various tissues. Monkeys injected with AAV2(beta-galF) (2.5×10^{10} gc) were sacrificed at 2 days or 3 months after the injection

Tissue	Monkey				
	#1 (Mock)	#2 (2d)	#4 (3m)	#5 (3m)	#3 (3m)[1)]
Cerebrum	−	+	+	−	−
Cerebellum	−	+	+	+	+
Bone marrow	−	++	+	−	−
Retina	−	−	−	−	ND
Skin	−	−	+	−	+
Muscle	−	−	−	−	−
Trachea	−	+	−	+	+
Lung	−	++	−	−	+
Heart	−	−	+	−	−
Liver	−	++	−	−	+
Gallbladder	−	++	+	−	+
Pancreas	−	+	+	+	−
Spleen	−	++++	++	−	+++
Esophagus	−	+	−	−	−
Stomach	−	+	−	−	+
Jejunum	−	ND	−	+	+
Ileum	−	+	+	+	−
Colon	−	+	+	+	ND
Kidney	−	−	+	−	+
Adrenal gland	−	−	−	−	−
Bladder	−	+	−	ND	+
Tonsil	−	+++	+	−	+
Thymus	−	+	−	−	−
Parotid gland	−	+	−	−	−
Submandibular gland	−	+	−	−	−
Thyroid gland	−	++	+	−	+
Axillary lymph node	−	+++	+	−	−
Hilar lymph node	−	+	ND	−	+
Mesenteric lymph node	−	++	−	−	+
Iliac lymph node	−	++	ND	ND	ND
Inguinal lymph node	−	+	+	−	+
Testis/Ovary	−	+	−	+	+
Epididymis/Uterus	−	+	ND	+	−

[1)]: #3 was received second injection of AAV2(beta-galF) (5×10^{10} gc) at 60 days after the first injection. (−), <10^2 gc/0.5 μgDNA; (+), 10^2-10^3 gc/0.5 μgDNA; (++), 10^3-10^4 gc/0.5 μgDNA; (+++), 10^4-10^5 gc/0.5 μgDNA; (++++), >10^5 gc/0.5 μgDNA; (ND), Not done.

Distribution of AAV2(EGFPtub) in cynomolgus monkeys and expression of EGFPtub: In Experiment II, 2.5×10^{11} gc of AAV2(EGFPtub) (Fig. 1) was administered into four monkeys (#6, 7, 8, 9) intravenously into the femoral vein, and the monkeys were sacrificed at 3 months pi (Tables 1 and 3). The vector DNA in various tissues was examined by similar procedures to those used in Experiment I. With some variation from monkey to monkey, high levels of the vector DNA (>10^3 gc/0.5 μg DNA) tended to be detected in the spleen, liver, gallbladder, tonsils, and lymph nodes, and low levels of the vector DNA (<10^3 gc/0.5 μg DNA) were present in the cerebrum, bone marrow, muscle, trachea, lung, heart, pancreas, esophagus, colon, kidney, adrenal gland, bladder, and parotid gland. At 3 months after injection, the vector DNA was not detected in the blood samples. Therefore, we concluded that the vector DNA in these specimens was not derived from contamination with blood.

EGFPtub expression was detected in the axillary lymph nodes of monkeys #7, 8, and 9 (Fig. 3). Endogenous tubulin and EGFPtub proteins were extracted from the liver, spleen, tonsils, and axillary lymph nodes of the monkeys. The two proteins were readily co-purified and concentrated by a previously described method (15). The tubulin/EGFPtub complex extracted from approximately 10^7 cells was analysed by SDS-polyacrylamide gel electrophoresis followed by immunoblotting with a mixture of anti-EGFP and anti-alpha-tubulin antibodies. The tubulin/EGFPtub complex extracted from a newly produced HeLa cell clone expressing EGFPtub was used as a size-marker for endogenous tubulin and EGFPtub protein. Comparison with commercially available purified tubulin (Sigma-Aldrich) enabled us to estimate the approximate amounts of EGFPtub (Fig. 3A). Samples for immunoblotting (50 mg) contained approximately 10 to 20 ng of EGFPtub. Under these conditions, transgene expression was detected in 6 out of 23 axillary lymph nodes tested. No transgene expression was detected in the other tissues including the spleen and liver, in which the injected vector DNA was readily found, most likely because the analyzable volume of a single piece of tissue is limited. Therefore, it remains unclear whether the transgene was not expressed in most of the tissues or the cells expressing the transgene were escaped from the sampling.

Table 3. Experiment II: Detection of the vector genomes in the various tissues. Monkeys injected with AAV2(EGFPtub) (2.5×10^{11} gc) were sacrificed at 3 months after the injection

Tissue	Monkey			
	#6 (3m)	#7 (3m)	#8 (3m)	#9 (3m)
Cerebrum	+	−	−	−
Cerebellum	−	−	−	−
Spinal cord	−	−	−	−
Bone marrow	++	++	−	−
Skin	−	−	−	−
Muscle	++	++	−	−
Trachea	+	++	+	−
Lung	−	−	−	+
Heart	+	+	−	+
Liver	+++	+++	−	+
Gallbladder	+	+	−	+++
Pancreas	+	+	−	−
Spleen	++++	++++	++	+++
Esophagus	+	−	−	−
Stomach	−	−	−	−
Jejunum	−	−	−	−
Ileum	−	−	−	−
Colon	+	−	−	−
Kidney	+	−	+	+
Adrenal gland	+	−	−	++
Bladder	+	−	−	−
Tonsil	++	+	+++	++
Thymus	−	−	−	−
Parotid gland	−	−	−	++
Submandibular gland	−	−	−	−
Thyroid gland	−	−	−	−
Axillary lymph node	++	++	+	++
Hilar lymph node	++	++++	++	−
Mesenteric lymph node	++	+	+	−
Iliac lymph node	++	+++	++	−
Inguinal lymph node	+	++	+++	−
Testis/Ovary	−	−	−	−
Epididymis/Uterus	−	−	−	−

(−), <10^2 gc/0.5 μgDNA; (+), 10^2-10^3 gc/0.5 μgDNA; (++), 10^3-10^4 gc/0.5 μgDNA; (+++), 10^4-10^5 gc/0.5 μgDNA; (++++), >10^5 gc/0.5 μgDNA.

In Experiment III 1.0×10^{11} gc of AAV2(EGFPtub) (Fig. 1) was administered to four monkeys (#10, 11, 12, 13), as was done in Experiment II, and the vector DNA in various tissues was examined at 5 months pi (Table 4). The vector distribution was similar to that observed at 3 months pi, indicating the vector DNA was stably maintained in various tissues. The levels of vector DNA in the tissues were similar to those observed at 3 months pi (Experiment II).

Distribution of AAV2/10(EGFPatub) and AAV2/11 (EGFPbtub) in cynomolgus monkeys: Since the data in the several recent studies indicated that the AAVs of different serotypes have different tissue tropism, in Experiment IV, the AAV2/10 and AAV2/11 pseudotype vectors (Fig. 1) and the AAV2 vector were compared as to the vector DNA distribution pattern in monkeys (Table 5). The entire coding regions of

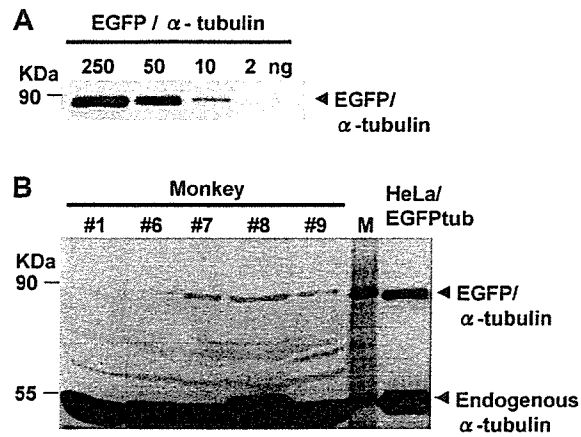

Fig. 3. Detection of transgene expression in monkey tissues. (A) Sensitivity of immunoblotting for fusion protein of EGFP and alpha-tubulin (EGFP/alpha-tubulin). The complex of endogenous tubulin and EGFP/alpha-tubulin was extracted from HeLa cells expressing EGFP/alpha-tubulin. The extracts were electrophoresed in a SDS-polyacrylamide gel and transferred to a nylon membrane. The EGFP/alpha-tubulin was detected with a mixture of anti-EGFP and anti-alpha-tubulin antibodies. The amount of EGFP/alpha-tubulin was estimated by the comparison with known amount of commercially available purified tubulin. (B) Expression of EGFP/alpha-tubulin in the lymph node of monkeys. The complex of endogenous tubulin and EGFP/alpha-tubulin was extracted from the axillary lymph node of monkeys, injected with mock inoculate (monkey #1) or AAV2(EGFPtub) (monkeys #6, 7, 8, and 9). The EGFP/alpha-tubulin was detected as described above.

AAV10 and AAV11 were recently isolated from cynomolgus monkeys, and the pseudotyped vectors were produced as previously described (12). To compare the distribution of the three vectors in the same monkey, AAV2(EGFPtub), AAV2/10(EGFPatub), and AAV2/11(EGFPbtub) were mixed together, and a mixture containing 1.0×10^{10} gc of each vector was administered intravenously to three monkeys (#15, 16, 17). One monkey (#14) received saline as a negative control. The PCR DNA derived from three vector genomes are distinguishable by measuring the sizes of DNA fragments produced by the digestion of the PCR DNA with *Hin*dIII, because the EGFP genes of AAV2/10(EGFPatub) and AAV2/11(EGFPbtub) have the *Hin*dIII site at different positions (Fig. 1). The vector inoculations did not induce any clinical symptoms, thus indicating that the AAV10 and AAV11 capsids exerted no acute toxicity. Serum samples were collected 1 week before and 1, 5, 9, and 11 weeks pi. Three monkeys (#14, 15, 16) were sacrificed at 3 months pi, and one monkey (#17) was sacrificed at 7 months pi.

The AAV2/10(EGFPatub) DNA was found primarily in lymphoid tissues such as the spleen and lymph nodes (Table 5). The levels of the AAV2/10(EGFPatub) DNA in the lymphoid tissues at 3 months pi (monkeys #15 and 16) were similar to those at 7 months pi (monkey #17), suggesting that the vector genome was stably maintained. The AAV2/11 (EGFPbtub) DNA was similarly found in the lymphoid tissues of monkeys #15 and 17, but was not found in any tissues from monkey #16 (Table 5). Consistent with our previous observation that the vector DNA was not found in the liver of mice intravenously injected with the AAV2/11 pseudotyped vector (12), no AAV2/11(EGFPbtub) DNA was found in the livers of monkeys #15 and 17.

Table 4. Experiment III: Detection of the vector genomes in the various tissues. Monkeys injected with AAV2(EGFPtub) (1.0×10^{11} gc) were sacrificed at 5 months after the injection

Tissue	Monkey			
	#10 (5m)	#11 (5m)	#12 (5m)	#13 (5m)
Cerebrum	–	–	–	–
Cerebellum	–	–	–	–
Bone marrow	–	–	–	+
Skin	–	–	–	–
Muscle	–	+	–	+
Trachea	–	–	–	–
Lung	+	+	–	+
Heart	+	+	–	–
Liver	++	+++	–	+++
Gallbladder	–	++	–	–
Pancreas	++	–	+	–
Spleen	++	++++	+++	+++
Esophagus	–	–	–	–
Stomach	–	–	–	–
Jejunum	–	–	–	–
Ileum	–	+	–	–
Colon	–	+	–	+
Kidney	–	+	+	+
Adrenal gland	–	+	–	+
Bladder	–	+	–	–
Tonsil	+	+	++	–
Thymus	–	+	–	+
Parotid gland	–	–	–	–
Submandibular gland	–	–	+	–
Thyroid gland	–	+++	–	–
Axillary lymph node	–	++	++++	+
Mesenteric lymph node	–	+	+	–
Iliac lymph node	–	+++	–	–
Inguinal lymph node	+	+++	++	–
Testis/Ovary	–	–	–	–
Epididymis/Uterus	–	+	–	–

(–), $<10^2$ gc/0.5 μgDNA; (+), 10^2-10^3 gc/0.5 μgDNA; (++), 10^3-10^4 gc/0.5 μgDNA; (+++), 10^4-10^5 gc/0.5 μgDNA; (++++), $>10^5$ gc/0.5 μgDNA.

Immune responses to the vectors varied from monkey to monkey. Since mouse anti-AAV2, AAV10, and AAV11 VP2 sera neutralized the AAV2, 10, and 11 vectors in a type-specific manner (12), it is very likely that the neutralizing activity of monkey antibody against AAV2, 10, and 11 is type-specific. Since it is possible that the monkeys had been infected with AAVs immunologically cross-reactive to AAV2, 10, and 11, the pre-administration serum obtained 1 week before the inoculation was considered as the baseline antibody titer (Fig. 4). Monkey #15 developed anti-AAV11 and low-level anti-AAV10 neutralizing antibodies, but did not develop anti-AAV2 antibody (Fig. 4), although similar levels of AAV2 (EGFPtub), AAV2/10(EGFPatub), and AAV2/11(EGFPbtub) DNAs were found in various lymphoid tissues (Table 5). The low level of anti-AAV11 neutralizing antibody that was present in the pre-administration serum was not found to inhibit the distribution of AAV2/11(EGFPbtub) (Table 5).

Monkey #16 developed anti-AAV2 and anti-AAV10 neutralizing antibodies, but did not develop anti-AAV11 antibody (Fig. 4). As was the case with monkey #15, the low level neutralizing antibody against AAV10 in the pre-administration serum (Fig. 4) did not inhibit the distribution of AAV2/10(EGFPatub) (Table 5). Since no anti-AAV11 neutralizing antibody was detected in the pre-administration serum of monkey #16, the absence of AAV2/11(EGFPbtub) DNA in monkey #16 (Table 5) could not be explained by the neutralization of the vector.

Monkey #17 responded to the three vector capsids and developed antibodies against AAV2, 10, and 11. It is likely that low doses of the vectors induced various immune responses of the monkeys against the vectors.

DISCUSSION

In this study, we intravenously administered AAV vectors (AAV2, AAV2/10, and AAV2/11) at a dose of 2×10^9 gc to 5×10^{10} gc/kg weight to cynomolgus monkeys, and we examined the behavior of the vectors and the responses of the monkeys. We assumed that intravenous injections at a relatively low dose of vector would mimic systemic conditions caused by targeted high-dose injections. We found that vector DNA persists for a long period of time, probably without replication, in various tissues, and in particular in the lymphatic tissues. We also demonstrated that the transgene is expressed in the axillary lymph nodes. These data are pertinent for the assessment of vector safety, although the status of the persisting vector DNA remains unclear, and the factors that regulate the transgene expression must still be investigated.

Following AAV2 vector inoculation, rapid excretion of the vector in the urine was very limited. By 1 week pi, the AAV2 vector DNA became undetectable in the circulating blood. At 2 days pi, the vector DNA was readily detected in the lymphoid tissues, especially in the spleen (Table 2). The vector DNA was detected at lower levels in the brain, lung,